We are IntechOpen, the world's leading publisher of Open Access books Built by scientists, for scientists

6,900
Open access books available

185,000
International authors and editors

200M
Downloads

Our authors are among the

154
Countries delivered to

TOP 1%
most cited scientists

12.2%
Contributors from top 500 universities



WEB OF SCIENCE™

Selection of our books indexed in the Book Citation Index in Web of Science™ Core Collection (BKCI)

Interested in publishing with us?
Contact book.department@intechopen.com

Numbers displayed above are based on latest data collected.
For more information visit www.intechopen.com



13

Photoferroelectric Nanowires

Marian Nowak
Silesian University of Technology
Poland

1. Introduction

The presented in (Gruverman & Kholkin, 2006; Scott, 2006) advances in the quickly developing field of nanoscale ferroelectrics are made because they are important for many applications as well as for the fundamental physics questions. This review summarizes results of investigations of nanowires of antimony sulfoiodide (SbSI) -type materials (i.e. SbSI, antimony selenoiodide (SbSeI), and antimony sulfoselenoiodide ($SbS_xSe_{1-x}I$)). This class of materials represents the semiconducting ferroelectrics (Fridkin, 1980; Gerzanich et al., 1982; Dittrich et al., 2000) known also as photoferroelectrics (Fridkin, 1979). Since photons in a semiconductor generate excess free carriers, and induce a change of its electronic state, one may observe a lot of interesting phenomena in these materials. Obviously, the presented new materials as the other one-dimensional semiconductor nanostructures (Xia et al., 2003) should receive considerable attention from the scientific and engineering communities due to their potentially useful novel electronic and optical properties.

The first description of the synthesis of SbSI was given almost two centuries ago (Henry & Garot, 1824) but the crystal structure of this and the other ternary chalcohalides formed from the group 15-16-17 elements was established much later (Dönges, 1950). However, the intensive investigation of SbSI started after discoveries of its photoconductivity (Nitsche & Merz, 1960) and its ferroelectric properties (Fatuzzo et al., 1962). An unusually large number of interesting properties of SbSI has been found. Among them there are the pyroeletric, pyro-optic, piezoeletric, electromechanical, electrooptic and nonlinear optical effects. Due to these properties it is an attractive and suitable material for thermal imaging, light modulator, ferroelectric field effect transistor, gas sensors, piezoelectric elements used in certain types of electromechanical sensors and actuators, temperature auto stabilized nonlinear dielectric elements (TANDEL), time-controlling devices and other applications (see e.g. Refs. in (Nowak et al., 2008; Nowak et al., 2009d). The SbSI is also taken into consideration as a valuable material for photonic crystals (see Refs. in (Nowak et al., 2008)).

It should be noted that quaternary compounds formed as solid solutions from the group 15-16-17 elements possess additional very interesting feature: their energy band gaps and physical properties are tailored with stoichiometric composition. For example, in $SbS_{1-x}Se_xI$ mixed crystals the strong monotonous decrease of the Curie temperature with the increase of Se content had been observed (Nitsche et al., 1964).

Being a promising material with potential applications, SbSI-type materials were synthesized in a variety of ways and prepared in different forms: bulk crystals, polycrystalline samples, ceramics, and thin-films (see e.g. Refs. in (Nowak et al., 2008;

Source: Nanowires Science and Technology, Book edited by: Nicoleta Lupu,
ISBN 978-953-7619-89-3, pp. 402, February 2010, INTECH, Croatia, downloaded from SCIYO.COM

Nowak et al., 2010b). The attempts have been made to produce SbSI nanocrystals. The SbSI quantum dots were synthesized in the Na_2O-B_2O_3-SiO_2 organic modified silicates matrix by the sol-gel technique (Yuhuan et al., 1999). Nanocrystals of SbSI were produced also in organically modified TiO_2 glass (Hui et al., 2000; Yuhuan et al., 2001; Hui et al., 2002). The SbSI nanorods were prepared by hydrothermal method (Wang et al., 2001). It should be mentioned that the SbSI nanocrystals were obtained by ball milling (Gomonnai et al., 2003; Voynarovych et al. 2003; Gomonnai et al. 2004), too. Recently, the ultrasound irradiation was applied to induce the 1D growth of nanowires of ternary and quaternary chalcohalides formed from the group 15-16-17 elements. Up to now this sonochemical technique was established for direct preparation of SbSI (Nowak et al. 2008), SbSeI (Nowak et al. 2009b), and $SbS_{1-x}Se_xI$ (Nowak et al. 2010b) nanowires. It was also applied for growing SbSI in multi-walled carbon nanotubes (CNTs) (Nowak et al. 2009c).

2. Sonochemical preparation of photoferroelectric nanowires

In sonochemistry powerful ultrasound is used to stimulate chemical reactions and physical changes in liquids. It is successfully applied to produce nano-structured metals, alloys, oxides, carbides and sulfides, or nanometer colloids (Gedanken, 2004). Ultrasound irradiation can be used at room temperature and ambient pressure to promote heterogeneous reactions that normally occur only under extreme conditions of hundreds of atmospheres and degrees (Li et al., 1999). An acoustic pressure wave consists of alternate compressions and rarefactions in the transmitting medium along the wave propagation direction. When a large negative pressure is applied to a liquid, intermolecular van der Waals forces are not strong enough to maintain cohesion and small cavities or gas-filled microbubbles are formed. The rapid nucleation, growth and implosive collapse of these micrometer-scale bubbles constitutes the phenomenon of cavitation. According to the thermal ''hot spot'' theory, extreme local temperatures and pressures are produced inside the cavitating bubbles and at their interfaces when they collapse. The effective temperature of the resulting transient, local ''hot spots'' was estimated to be in the range of 5200±650 K (Suslick et al., 1986). Assuming such value, the pressure during collapse, as inferred from the van der Waals equation, would be approximately 1700 atm. These exceptional local conditions can be used to generate nanostructured SbSI-type materials.

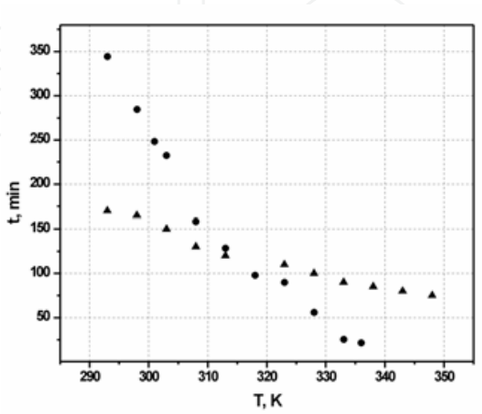


Fig. 1. Comparison of duration of the sonochemical synthesis of SbSI in ethanol (▲) and methanol (●) as a function of temperature of the bath (after (Starczewska et al., 2009))

The SbSI, SbSeI, and $SbS_{1-x}Se_xI$ were prepared sonically from the constituents (the elements antimony, sulfur, selenium and iodine). Ethanol or methanol served as the solvent for this reaction. In a typical procedure, the elemental mixture with appropriate stoichiometric ratio and with total mass of a few grams was immersed at room temperature and ambient pressure in 8-40 ml of alcohol, which was contained in a 54 ml Pyrex glass cylinder of 20 mm inside diameter. The vessel was closed during the experiment to prevent volatilization of the precipitant in long time tests. The cylinder was partly submerged in water in an ultrasonic reactor (frequency 35 kHz, with 80 W electrical power and 2 W/cm^2 power density guaranteed by the manufacturer). The sonolysis was carried out at various temperatures (Fig. 1) but usually at 323 K. The level of the alcohol slurry inside the tube was the same as that of the water in the sonication bath, in order to obtain reproducible sonochemical yields.

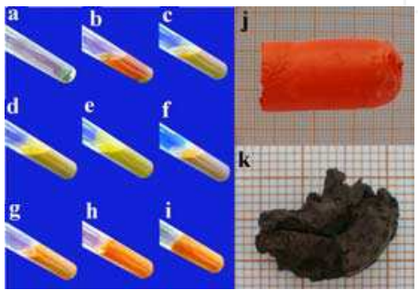


Fig. 2. Change of color and consistence during the sonication of Sb, S and I in ethanol (a-i) and the obtained SbSI (j) as well as SbSeI (k) xerogels (a- dry elements before the process; b- test-tube with the elements in ethanol at the beginning of the process; c- after 20 sec. of sonication, T=323 K; d- 3 min.; e- 6 min.; f- 26 min.; g- 48 min.; h- 75 min.; i- SbSI ethanogel solidified after 110 min.) (after (Starczewska et al., 2008; Nowak et al., 2010c))

During the sonications sols were formed (Fig. 2). The oxidation-reduction potential Eh=0.15 V and negative logarithm of the activity of the hydrogen ion pH=1.2 of the Sb-S-I-ethanol sol after 20 minutes of sonication was measured (Nowak et al., 2010b). It was observed that the color of the slurry changed gradually indicating the growth process of the SbSI, SbSeI and $SbS_{1-x}Se_xI$. For example, in the case of SbSI the color changed from red (before sonication) into olive, green, yellow and then into red-orange after 45 min of sonication, indicating the growth process of SbSI nanorods (Fig. 2). To control this process, measurements of optical diffusive reflectance $R_d(\lambda)$ of the sample were performed. It was assumed that the sonochemical process is finished when the spectral characteristics of $R_d(\lambda)$ do not change with time. It is noteworthy that the SbSI, SbSeI and $SbS_{1-x}Se_xI$ sols converted into gels after relatively short sonications (see e.g. Fig. 1). Their colors depended on the molar composition and changed from red-orange for SbSI to brown for SbSeI (Fig. 2). The time necessary for complete gelation depends on the molar composition, the used solvent, and the temperature of the water in the ultrasonic bath (see e.g. Fig. 1). The temperature dependences of acoustic impedances do not allow to explain the differences in the observed times of ultrasonic synthesis of SbSI gels in ethanol and methanol. Probably, these differences are due to different temperature dependences of solubilities of the components in the growth of SbSI nanowires in ethanol and methanol.

When the alcohol was evaporated from the SbSI or SbSeI gels during the drying, the relatively big (of a few cm^3 volume), rigid but brittle samples of a so-called xerogels were obtained (see e.g. Fig. 2). During this process the observed SbSeI syneresis was a few times

larger (Nowak et al., 2009b) than the about 40 % decrease of volume of the dried SbSI ethanogel (Nowak et al., 2008). It means that the SbSeI ethanogel is much less rigid than the SbSI ethanogel. The SbSeI xerogel is also more brittle than the SbSI xerogel. The masses of the samples after drying were practically equal to the sum of masses of the elements used for the sonochemical synthesis.

Recently (Nowak et al., 2010b), to extract the eventual remaining substrates the $SbS_{1-x}Se_xI$ gels were eight times rinsed with ethanol and centrifuged. Each time the liquid above the sediment was replaced with pure ethanol to wash the precipitates. At the end the centrifuged product was covered by colorless ethanol. As in the cases of sonochemical preparation of other nanocrystalline products, e.g. SbSI and SbSeI, this alcohol was evaporated in air at 313 K, so the $SbS_{1-x}Se_xI$ xerogels were obtained.

In (Nowak et al., 2009c) the SbSI was prepared ultrasonically in CNTs from the constituents (the elements Sb, S and I). Methanol served as the solvent for this reaction. In a typical procedure, the elemental mixture with stoichiometric ratio of e.g. 0.380 g Sb, 0.099 g S and 0.394 g I, was immersed with 0.282 g of CNTs in 40 ml absolute methanol. The used experimental set up and the applied procedure were the same as the described for sonochemical preparation of alone SbSI-type nanowires. The sonication was continued for 3 h at 323 K. When it was finished a dark sol was obtained. It was centrifuged to extract the products. Then the liquid above the sediment was replaced with pure methanol to wash the precipitates. The centrifugation and washing were performed 5 times. At the end methanol was evaporated from the sample and a brown-purple CNTs filled with SbSI were obtained.

3. Mechanism of sonochemical preparation of photoferroelectric nanowires

3.1 Process route of SbSI-type nanowires growing

The transient high-temperature and high-pressure field produced during ultrasound irradiation provide a favorable environment for the 1D growth of the SbSI-type nanocrystals, though the bulk solution surrounding the collapsing bubbles is at ambient temperature and atmospheric pressure. It seems that $SbS_{1-x}Se_xI$ as well as SbSI and SbSeI belong to the many solid materials (Xia et al., 2003) that naturally grow into 1D nanostructures, and this habit is determined by the highly anisotropic bonding in the crystallographic structure. The probable reaction route of $SbS_{1-x}Se_xI$ synthesis and the mechanism of formation of its nanowires using elemental Sb, S, Se and I in the presence of ethanol under ultrasonic irradiation can be summarized as follows (Nowak et al., 2010b):

1. iodine, I_2, dissolved in ethanol reacts with antimony and forms the antimony triiodide, SbI_3, also dissolved in ethanol

$$2Sb+3I_2 \rightarrow 2SbI_3 \quad (1)$$

2. dehydrogenation, dehydration as well as decomposition of ethanol in or close to the cavitation bubbles leads to the formation of hydrogen and water as the main products (Gutiĕrrez & Henglein, 1988; Mizukoshi et al., 1999)

$$C_2H_5OH \leftrightarrow C_2H_4O+H_2,\ C_2H_5OH \leftrightarrow C_2H_4+H_2O,\ C_2H_5OH \leftrightarrow C_2H_5O+H \quad (2)$$

3. the sonolysis of water yields the $H^{\bullet}$ and $OH^{\bullet}$ radicals

$$H_2O\ ))) \ H^{\bullet}+OH^{\bullet} \quad (3)$$

4. the ultrasonic irradiation facilitates the reduction of chalcogens (S and Se) to the active forms of S^{-2} and Se^{-2} (see e.g. Refs. in (Li et al., 1999; Gedanken, 2004)) that react with the in-situ generated H• radicals forming H_2S and H_2Se (Li et al., 2003)

$$S+2H^{\bullet}\rightarrow H_2S,\ Se+2H^{\bullet}\rightarrow H_2Se \tag{4}$$

5. the released H_2S and H_2Se react with SbI_3 to yield SbSI and SbSeI molecules

$$SbI_3+H_2S\rightarrow SbSI+H_2+I_2 \tag{5a}$$

$$SbI_3+H_2Se\rightarrow SbSeI+H_2+I_2 \tag{5b}$$

6. the created SbSI and SbSeI molecules, under the microjets and shockwaves formed at the collapse of the bubbles are pushed towards each other and are held by chemical forces. Therefore, the nuclei of SbSI, SbSeI and $SbS_{1-x}Se_xI$ are formed as a result of the interparticle collisions (see e.g. (Gedanken, 2004));
7. the freshly formed nuclei in the solution are unstable and have the tendency to connect with each other and self-assemble to form double chain-type structures. These $[(SbSI)_\infty]_2$, $[(SbSe)I)_\infty]_2$ or $[(SbS(Se)I)_\infty]_2$ structures consist of two chains related by a two-fold screw axis and linked together by a short and strong Sb–S (Gerzanich et al. 1982) or Sb-Se bonds (Voutsas & Rentzeperis, 1986). High temperature, local turbulent flow associated with cavitation, and acoustic streaming greatly accelerate mass transport in the liquid phase and are favorable for the self-assembly of the SbSI, SbSeI and $SbS_{1-x}Se_xI$ nuclei;
8. the SbSI, SbSeI or $SbS_{1-x}Se_xI$ chains can be readily crystallized into 3D lattice of nanowiskers through van der Waals interactions. Induced by this structure, crystallization tends to occur along the c-axis, favoring the stronger covalent bonds over the relatively weak, inter-chain van der Waals forces (Molnar et al., 1965). Thus, this solid material has a tendency to form highly anisotropic, 1D structures;
9. the aggregated SbSI, SbSeI or $SbS_{1-x}Se_xI$ nanowires produce larger species. Ultrasound can also promote chemical reaction and crystal growth by mixing heterogeneous phases involving the dispersion of an insoluble solid reactant, e.g. SbSI, in a liquid medium. During the sonication time, the surface state of the nanowires might change: the dangling bonds, defects, or traps decrease gradually, and the species grow until the surface state becomes stable; surface corrosion and fragmentation by ultrasound irradiation affect the formation of regular nanowires.

Compounds of low volatility, which are unlikely to enter cavitation bubbles, experience a high-energy environment resulting from the pressure changes associated with the propagation of the acoustic wave or with shock waves; or they can react with radical species generated by sonolysis of the solvent. A nanocrystalline product is expected if the reaction takes place at the interface (Suslick et al., 1986). In the presented case, the reagents Sb, S and Se are much less volatile than the ethanol and the iodine, so they stay in the interfacial region of the cavitation bubbles to yield SbSI, SbSeI or $SbS_{1-x}Se_xI$ nanowires. The fine crystallinity of the products, which was confirmed by the HRTEM and SAED results (chapter 4), strongly supports this hypothesis.

The reactions (5a) and (5b), describing the synthesis of SbSI, SbSeI and $SbS_{1-x}Se_xI$, were used in different methods of preparation of bulk SbSI-type crystals, i.e.: by reaction of dry H_2S with dry heated SbI_3, by passing gaseous H_2S through the solution of SbI_3, by mixing H_2S

aqueous solutions with SbI_3 solution in HI (modification included the use of thioacetamide to generate in-situ the H_2S), by hydrothermal synthesis with $(NaH_2)_2CS$ or Na_2S used to generate in-situ the H_2S and with Na_2Se used to generate in-situ the H_2Se (see Refs. in (Nowak et al., 2010b)). The reaction (5a) was also used for the preparation of SbSI quantum dots in borosilicate gel (Yuhuan et al., 1999). According to (Popolitov & Litvin, 1970) formation of SbSI and SbSeI chains in solutions with pH<7 may be associated with ceaseless serial linking of hypothetical $[Sb_2I_2(H_2S)_4^{4-}]$ or $[Sb_2I_2(H_2Se)_4^{4-}]$ type complexes.

Solid solubility is a feature of many metallic and semiconducting systems, being favored when the components have similarities in crystal structure and atomic (ionic) diameter as the SbSI and SbSeI (see e.g. the Refs. in (Voutsas & Rentzeperis, 1986)). Therefore, the homogeneous $SbS_{1-x}Se_xI$ solid solutions exist. It has been established in powder X-ray diffraction of bulk crystals (Spitsyna et al., 1975; Voutsas & Rentzeperis, 1986) that $SbS_{1-x}Se_xI$ is obtained by statistical substitution of S atoms by Se. The fact that $SbS_{1-x}Se_xI$ forms a continuous solid solution has been proved by investigations of its optical transmission (Pouga et al., 1973). It is obvious, that the ultrasound irradiation provides appropriate conditions for statistical substitution of S and/or Se atoms in the $SbS_{1-x}Se_xI$ crystal structure. Of considerable importance is the increase in entropy associated with the formation of a disordered solid solution from the S and Se components random arranged in the matrix.

The sonochemical formation of SbSI nanowires is accompanied with the formation of other species, e.g. iodine can be sonochemically oxidized to triiodide (I_3^-) by OH• radicals produced during cavitation (Entezari & Kruus, 1996). However, the oxidative power of the I_3^- ion is lower than that of iodine molecules, I_2, itself (Lindsjö, 2005). So, the I_3^- seems to be not essential for the presented sonochemical preparation of $SbS_{1-x}Se_xI$.

It is well known that the liquid used during sonochemical preparation of nanomaterials strongly affects the yield of the sonochemical process and the properties of the produced material. The sonication depends on such properties of the liquid as e.g. the viscosity, surface tension, vapor pressure and sound speed. Methanol has greater vapour pressure and evaporation rate than ethanol but smaller decomposition rate during sonolysis (Mizukoshi et al., 1999). However, one should take into account not only the ultrasonical properties of the liquid. It was confirmed experimentally (Lebedev et al., (2003) that the mechanisms of interaction with crystal surface of the ions (e.g. HS^-) solvated e.g. by alcohol molecules and water are fundamentally different, because the chemical properties of the ions in solution can be strongly modified by the surrounding solvation shells. The solute reactivity depends on the following solvent's properties: dielectric constant, dipole moment, molecule polarizability, etc. The variation in the dielectric constant leads to a change in the nucleophilic properties of the reacting ions during bond formation. Such a variation can affect the charge transfer between bonding atoms, the bond length, and the covalent character of bonding (Lebedev et al., (2003).

3.2 Filling of CNTs with SbSI nanowires

As in the case of alone SbSI-type nanowires, the transient high-temperature and high-pressure field produced during ultrasound irradiation provide a favorable environment for the growth of SbSI nanocrystals from elements inside multi-walled CNTs in methanol, though the bulk solution surrounding the collapsing bubbles is at ambient temperature and atmospheric pressure. It was suggested in (Nowak et al., 2009c) that the filling is induced via capillarity. Hence, the reaction route presented above remains valid for this case. Discussion

of the crystal habit, the anisotropy of growth kinetics, and the critical role of unusual chain-type structure of SbSI played in the formation of the nanowires was presented above. The application of sonochemistry to prepare CNTs filled with SbSI is also justified by the fact that ultrasonication is often used in an attempt to cut the outer caps of CNTs (Eletskii, 2004).

4. Morphology, composition and crystal structure of SbSI-type nanowires

The scanning electron microscope (SEM) micrographs of SbSI xerogels obtained after drying the SbSI gels sonochemically prepared in ethanol and methanol as well as xerogels of SbSeI and $SbS_{0.5}Se_{0.5}I$ sonochemically prepared in ethanol (Fig. 3) show that morphologies of the SbSI-type xerogels are very similar. In all cases the samples existed as a porous gels composed of nanowires. It was found that the SbSI nanocrystals amounts only 4.7 % of volume of the sonicated SbSI xerogel (Nowak et al., 2008). The surface areas of the sonochemically prepared SbSI and SbSeI were estimated as about 75 m^2/g (Nowak et al., 2008) and 14÷34 m^2/g (Nowak et al., 2009b), respectively.

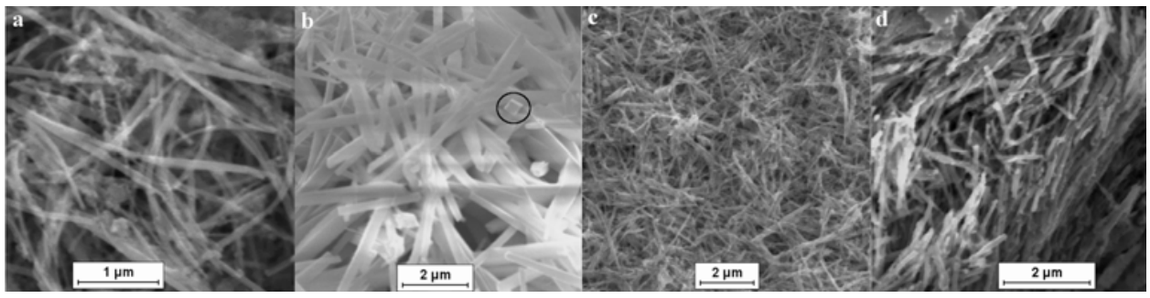


Fig. 3. Typical SEM micrographs of xerogels of SbSI sonochemically prepared in ethanol (a after (Starczewska et al., 2008)) and methanol (b after (Starczewska et al., 2009)) as well as xerogels of SbSeI (c after (Nowak et al., 2009b)) and $SbS_{0.5}Se_{0.5}I$ (d after (Nowak et al., 2010b)) sonochemically prepared in ethanol

The lateral dimensions of the SbSI nanowires produced sonochemically in methanol were found in wider range (10-300 nm (Starczewska et al., 2009)) than the ones of SbSI nanowires in ethanogel (10-50 nm (Nowak et al., 2008)). The SbSeI ethanogel (Nowak et al., 2009b) was composed of nanowires with average lateral dimensions of 20-50 nm. The $SbS_{1-x}Se_xI$ nanowires described in (Nowak et al., 2010b) had lateral dimensions of 10-50 nm. The average lengths of the SbSI, SbSeI, and $SbS_{1-x}Se_xI$ nanowires produced in ethanol and methanol were very similar (the lengths were up to several micrometers). Taking into account the mechanical properties mentioned in the last chapter, it was concluded (Nowak et al., 2009b) that the SbSeI nanowires are connected each other with much weaker forces than the SbSI ones. However, the crosslinking of the nanowires in SbSI-type xerogels still needs evaluation.

Circle in Fig. 3b marks rhomboidal cross section of one of the wider SbSI nanowires. The lateral dimensions of this nanowire are equal 280(4) nm, 263(7) nm, 294(4) nm and 252(3) nm. The angles between the appropriate surfaces are equal 92.7(6)°, 86.3(5)°, 91.3(5)° and 89.7(7)°. If one assumes that the observed nanowire is oriented perpendicularly to the figure, these values correspond to the angles between the (100) and (010) surfaces of bulk SbSI crystals (Starczewska et al., 2009).

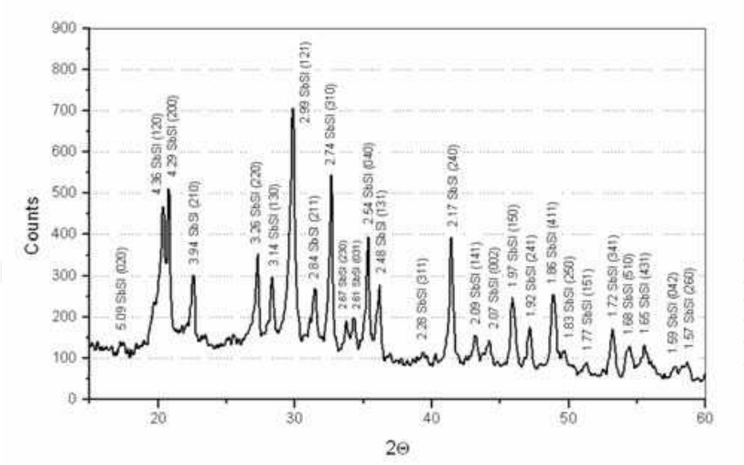


Fig. 4. The powder XRD pattern of orthorhombic phase of dried SbSI ethanogel at T=298 K (after (Nowak et al., 2008)

The reported powder X-ray diffraction (XRD) patterns of the SbSI-type gels prepared by the sonochemical method (see e.g. Fig. 4) indicated that the products were obtained with high purity and well crystallized. The crystal structure of SbSI ethanogel (Nowak et al. 2008) was well described by the *Pnam* crystal symmetry that is appropriate for the paraelectric bulk SbSI. The XRD investigations of SbSI sonochemically produced in methanol showed the coexistence of phases with $Pma2_1$ and *Pnam* crystal symmetry, hence the coexistence of ferroelectric and paraelectric domains (Starczewska et al., 2009). The values of the determined cell parameters are given in Table 1. It should be underlined that these lattice parameters are very close to the data reported for bulk SbSI (Dönges, 1950; Kikuchi et al., 1967). Probably, the XRD data obtained for SbSI methanogel at 298 K represent a structure of just below or very near the transition temperature. The coexistence of the ferroelectric and paraelectric phases of bulk SbSI near the Curie point was discussed in (Starczewska et al., 2009). From the differences in XRD data, it was concluded (Starczewska et al., 2009) that SbSI gels produced sonochemically in methanol and ethanol can have different Curie temperatures. The reason for this can be the differences in solvation processes in ethanol and methanol.

Liquids used during sonication	Phases and cell parameters determined in the case of SbSI nanowires sonicated in different liquids		
	Ethanol [a)]	Methanol [b)]	
Phases	Pnma	*Pnma*	$Pma2_1$
a , nm	0.858	0.8587(3)	0.8473(6)
b , nm	1.017	1.0190(6)	1.0478(5)
c , nm	0.414	0.4146(7)	0.4247(8)

Table 1. Phases and cell parameters determined at temperature 298 K for sonochemically prepared SbSI ([a)]- after (Nowak et al., 2008); [b)]- after (Starczewska et al., 2009)

All diffraction peaks in XRD pattern of sonochemical prepared SbSeI (Nowak et al., 2009b) were indexed to be a pure orthorhombic phase for SbSeI with the cell constants a=0.86862(9) nm, b=1.0.3927(3) nm, and c=0.41452(9) nm very close to the data reported for bulk SbSeI

crystals (Voutsas & Rentzeperis, 1982). However, the XRD patterns (Fig. 5) of $SbS_{1-x}Se_xI$ xerogels prepared by the sonochemical method (Nowak et al., 2010b) suggested the presence of additional phase. The red vertical line in Fig. 5 indicates the position of the main peak observed in the XRD pattern of antimony subiodide (Sb_3I) described in (Nowak et al., 2010d). Therefore, one can conclude that the Sb_3I can be present in $SbS_{1-x}Se_xI$ samples prepared sonochemically from the elemental Sb, S, Se and I in ethanol.

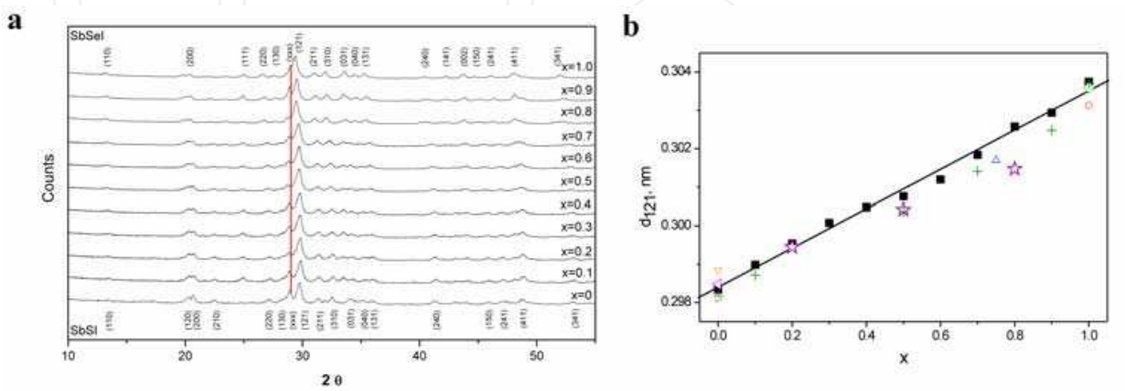


Fig. 5. (a) Influence of molar composition on the powder XRD patterns of orthorhombic phase of $SbS_{1-x}Se_xI$ nanowires (after (Nowak et al., 2010b)); (b) The distance between (121) planes determined from the diffraction peak vs. the Se concentration in $SbS_{1-x}Se_xI$ nanowires (■-(Nowak et al., 2010b); ○- (JCPDS Card 76-1354)); ◇- (JCPDS PDF 01-075-1723); △- (JCPDS PDF 01-072-2366); ◁ - (JCPDS Card 74-2245; JCPDS Card 74-2246; JCPDS Card 74-1195; JCPDS Card 74-1196, 2000; JCPDS Card 74-2244; JCPDS Card 75-0781; JCPDS Card 88-0985); (▽- JCPDS Card 74-2210); ✯- (Spitsyna et al., 1975); + - (Belayev et al., 1970); ▷- (JCPDS Card 21-0050); black line represents the least square fitted linear dependence (6)) (after (Nowak et al., 2010b))

Positions of XRD peaks depend on the molar composition of investigated $SbS_{1-x}Se_xI$ xerogel (Figs. 5a). The distances between (121) planes (determined from the diffraction peaks) were well fitted (Fig. 5b) by a linear function of the molar composition of $SbS_{1-x}Se_xI$ nanowires

$$d_{121}(x)=A_{121}+B_{121}\cdot x \tag{6}$$

where A_{121}=0.2984(1) nm, B_{121}=0.00511(16) nm. The obtained results are well compared to the bulk values of d_{121} reported for different compositions of $SbS_{1-x}Se_xI$ (Fig. 5b).

Typical transmission electron microscopy (TEM) image of an individual needle-shaped nanowire from sonochemically prepared SbSI-type xerogel is presented in Fig. 6a. The selected area electron diffraction (SAED) pattern (inserted at the upper left corner of Fig. 6a) of this nanowire indicates its good single-crystalline structure appropriate for the orthorhombic structure of bulk SbSI-type crystals (Voutsas & Rentzeperis, 1986). Figure 6b presents TEM image of an individual multiwalled CNT filled sonochemically with SbSI in methanol. The corresponding SAED (Fig. 6b) recorded on the end of this CNT indicates the interplanar spacings appropriate for CNTs as well as SbSI crystals (see Table 2). The TEM of a relatively thick CNT sonochemically filled with SbSI reveal that the product consists of coaxial nanocables (Fig. 6c). The lateral dimensions of the nanocables were in the range from 30 to 200 nm, and their lengths reached up to several micrometers (Nowak et al., 2009c).

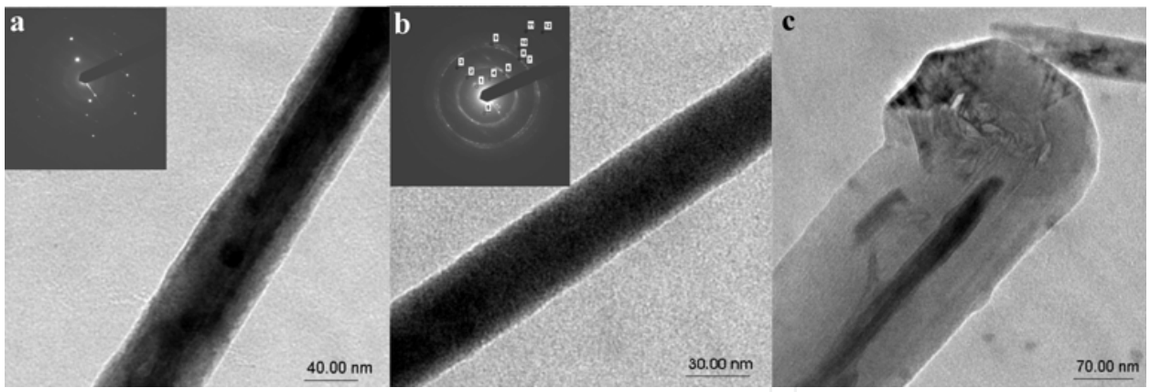


Fig. 6. Typical TEM images of (a) individual nanowire from sonochemically prepared $SbS_{0.75}Se_{0.25}I$ (after (Nowak et al., 2010b)), and relatively thin (b) and thick (c) multiwalled CNTs filled ultrasonically with SbSI in methanol (after (Nowak et al., 2009c)). The corresponding SAED patterns are inserted at the upper left corners of the images. The description of diffraction pattern presented in Fig. 6b is given in Table 2.

Sign	Results of the SAED d_{hkl} (nm)	Literature data			
		for C [a)]		for SbSI [b)]	
		d_{hkl} (nm)	(hkl)	d_{hkl} (nm)	(hkl)
1 reflex	0.4360	-- --	-- --	0.43402 0.42450	(120) (200)
4 reflex	0.3732	--	--	0.38465	(011)
5 reflex	0.3470	0.33950	(002)	0.35036	(111)
2 reflex	0.2189	0.21390	(100)	0.21663	(330)
6 reflex	0.2089	0.20402	(101)	0.20800	(002)
3 reflex	0.1446	-- --	-- --	0.14244 0.14244	(422) (531)
7 reflex	0.1190	-- --	-- --	0.12031 0.11960	(143) (181)
8 circle	0.1210	0.12350	(110)	--	--
9 circle	0.1155	0.11606 0.11464 0.11316	(112) (105) (006)	-- -- --	-- -- --
10 circle	0.1036	0.10425	(202)	--	--
11 circle	0.07874	0.07954	(122)	--	--
12 circle	0.07038	0.07720	(206)	--	--

Table 2. Comparison of interplanar spacings determined by SAED (Fig. 6B) of multiwalled CNT filled with SbSI ultrasonically in methanol with literature data for CNTs and SbSI bulk crystals ([a)]- after (JCPDS Card 75-1621); [b)]- after (JCPDS Card 74-0149)).

The good fitting of SAED patterns recorded on individual SbSI and SbSeI nanowires with the simulated diffraction patterns (Fig. 7) indicates that the sonochemically produced nanowires exhibit a single-crystalline structure with a preferred growth oriented along the [001] direction. The observed rod type morphology of the SbSI-type nanowires is possibly due to mentioned in chapter 3.1 the inherent chain-type structure and growth habit of them.

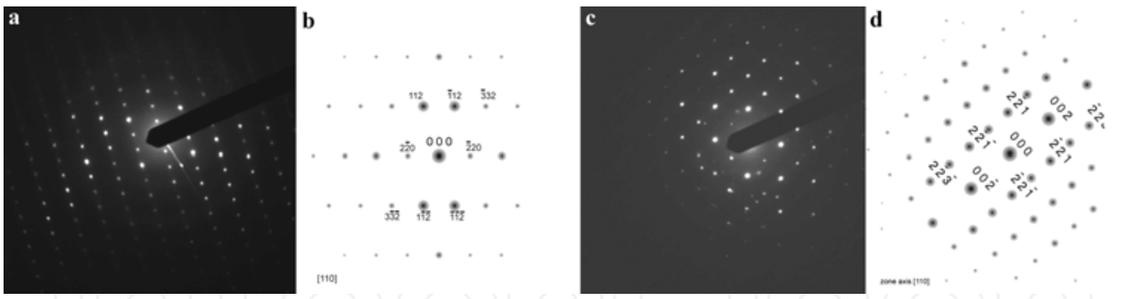


Fig. 7. SAED patterns of individual nanowires from sonochemically made SbSI methanogel (a- after (Starczewska et al. 2009)) and SbSeI ethanogel (c- after (Nowak et al., 2009b)) in the orientation close to the [110] zone axis with their simulated diagrams (b and d).

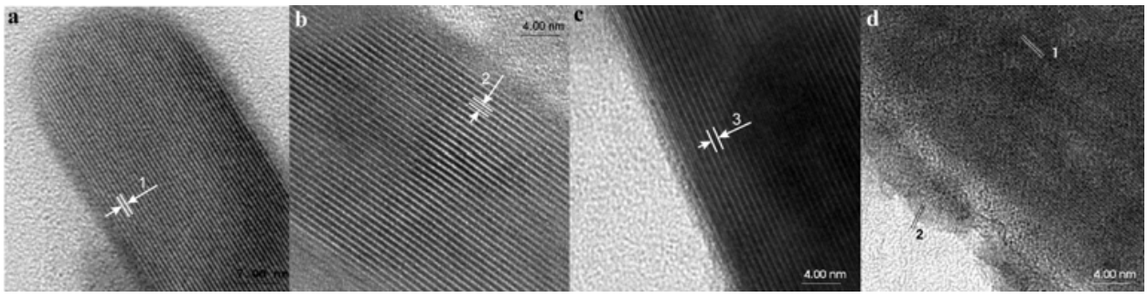


Fig. 8. Typical HRTEM images of individual nanowires from sonochemically prepared SbSI (a), $SbS_{0.75}Se_{0.25}I$ (b), SbSeI (c), and CNT filled with SbSI (d) (description in the text) (after (Nowak et al. 2010b) and (Nowak et al., 2009c))

Material	HRTEM investigations		Literature data for bulk crystals			
	Sign	d_{hkl} , nm	hkl	Material	d_{hkl} , nm	JCPDS Card
SbSI ethanogel	--	0.2962(22) [d]	(201)	SbSI	0.29540	74-1195
	(1) in Fig. 8a	0.654(8) [a]	(110)		0.65203	
	--	0.651(4) [b]				
	--	0.642(2) [c]				
	--	0.6556(22) [d]				
	--	0.6569(35) [e]				
SbSI methanogel	--	0.652(1) [f]				
	--	0.421(1) [f]	(001)		0.4100	
	--	0.377(1) [f]	(011)		0.38005	
$SbS_{0.75}Se_{0.25}I$	(2) in Fig. 8b	0.641(5) [a]				
SbSeI	(3) in Fig. 8c	0.661(7) [a]	(110)	SbSeI	0.66648	01-075-1723
	--	0.4467(9) [g]	(120)		0.4459	01-075-1723
CNT filled with SbSI	(1) in Fig. 8d	0.319(2) [h]	(220)	SbSI	0.32494	74-1195
	(2) in Fig. 8d	0.209(2) [h]	(100)	C	0.21390	75-1621

Table 3. Comparison of interplanar spacings evaluated from HRTEM images of SbSI-type nanowires and SbSI in an individual CNT with the data for bulk crystals ([a] (Nowak et al. 2010b); [b] (Nowak et al. 2008); [c] (Starczewska et al. 2008); [d] (Szperlich et al., 2009); [e] (Nowak et al., 2009e); [f] (Starczewska et al. 2009); [g] (Nowak et al., 2009b); [h] (Nowak et al., 2009c))

Figure 8 presents typical HRTEM images of sonochemically prepared SbSI-type nanowires and an individual CNT sonochemically filled with SbSI. They exhibit good crystalline and clear (110) lattice fringes parallel to the rod axis appropriate for the orthorhombic structure of bulk crystals. It indicates that the growth velocity in [001] direction is much larger than in the [110] one. Figure 8d shows also the lattice fringes of the CNT walls. Table 3 presents good conformity of the interplanar spacings evaluated from HRTEM images of SbSI-type nanowires with the XRD data of bulk crystals. The difference between d_{110} spacings reported in Table 3 for SbSI can be due to the little different positioning of the nanowires.
Figure 8 reveals that the SbSI-type nanowires are completely surrounded by fuzzy shells of practically constant thickness. The 5.4(2) nm and 6 nm thick fuzzy shells on the surfaces of SbSI nanowires sonochemically produced in ethanol has been reported in (Nowak et al., 2009e) and (Nowak et al., 2008), respectively. Similar but thinner fuzzy shell of about 2,77(8) nm was observed on the surface of SbSI nanowires sonochemically produced in methanol (Starczewska et al., 2009). The SbSeI nanowires sonochemically produced in ethanol had 7.1(2) nm thick fuzzy shell (Nowak et al., 2009b). This is probably due to the amorphous species adsorbed on the surface of the crystalline nanowires during their growing.

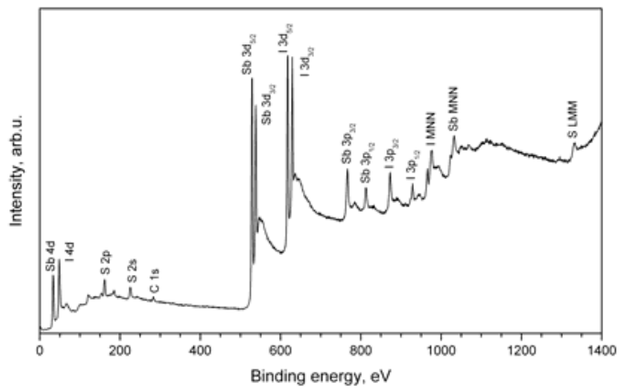


Fig. 9. XPS spectrum of SbSI ethanogel (after (Nowak et al., 2009e))

The presented in (Nowak et al., 2009e) results of the X-ray photoelectron spectroscopy (XPS) described just the surface layer of the SbSI nanowires sonochemically prepared in ethanol. They do not show any traces of O, OH groups, H_2O or other impurities, only a small amount of carbon (C 1s peak at 284.5 eV) is visible (Fig. 9). The carbon element may result from the rest gases in the vacuum chamber and/or can be bonded on the surface during preparation of the sample for XPS (Nowak et al., 2009e).

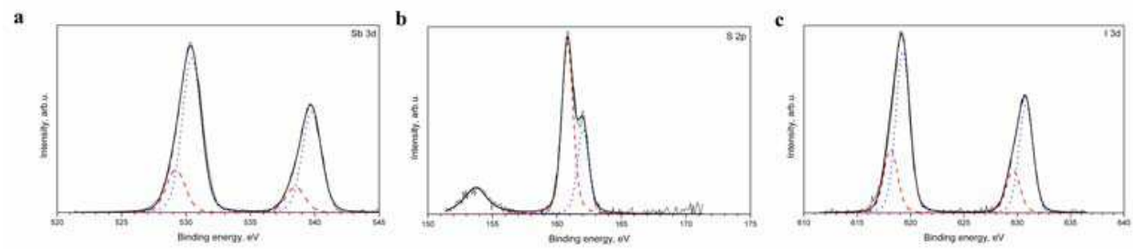


Fig. 10. XPS of the Sb 3d, S 2p and I 3d spin-orbit doublets from the SbSI ethanogel and Gaussian XPS contributions of them (after (Nowak et al., 2009e))

Table 4 shows binding energies of Sb, S and I in SbSI ethanogel prepared sonochemically. The overlapping peaks of S $2p_{3/2}$ and S $2p_{1/2}$ have been fitted with Gaussian functions (Fig. 10). Every line of spin-orbit doublets of the Sb 3d and I 3d states in SbSI nanowires, has been split into two Gaussian components (Fig. 10). Comparing parameters of these components (Table 5) with literature data, one can see that, the chemical shifts of binding energies of peaks in the XPS spectrum of SbSI ethanogel prepared sonochemically are different from those of bulk SbSI.

Material	Binding energy (eV)					
	Sb $3d_{5/2}$	Sb $3d_{3/2}$	S $2p_{3/2}$	S $2p_{1/2}$	I $3d_{5/2}$	I $3d_{3/2}$
SbSI nanowires[a)]	530.3	539.7	160.8	162.0	619.1	630.7
powdered SbSI crystals[b)]	529.5	538.9	161.2		618.8	630.3
(110) plane of single crystal at 293 K[c)]	529	538	161	162	618.2	629.2
Sb_3I nanoparticles[d)]	530.7	540.1	--	--	619.5	630.9
Pure elements[e)]	528.3	537.6	164.0	165.2	619.3	630.8

Table 4. Comparison of energies of peaks in the XPS spectrum of SbSI ethanogel prepared sonochemically with the data reported for single crystals of SbSI and Sb_3I nanoparticles ([a)]- (Nowak et al., 2009e); [b)]- (Ikemoto, 1981); [c)]- (Grigas et al., 2004); [d)]- (Nowak et al., 2010d); [e)]- (Moulder et al., 1995); calibrated to C 1s = 284.5 eV).

Material	Line	Chemical shift in comparison with binding energy in pure element (eV)					
		Sb		S		I	
		$3d_{5/2}$	$3d_{3/2}$	$2p_{3/2}$	$2p_{1/2}$	$3d_{5/2}$	$3d_{3/2}$
SbSI ethanogel[a)]	Total	+2.0	+2.1	-3.2	-3.2	-0.2	-0.1
	Main line	+2.2	+2.2	-3.1	-3.2	0.0	0.0
	Additional line	+0.9 (0.28)	+0.9 (0.26)			-1.2 (0.39)	-1.2 (0.39)
powdered SbSI crystals[b)]		+1.2	+1.26	~(-3.3)		-0.5	-0.5
(110) plane of SbSI crystal[c)]		+1		-3		-0.8	
SbSI crystals[d)]		+1		-3		-0.8	
SbSI crystals[e)]		+0.8		-3		-0.8	
Sb_3I nanoparticles[f)]	Total	+2.4	+2.5	--	--	+0.1	+0.1
	Main line	+2.6	+2.6	--	--	+0.2	+0.2
	Additional line HE	+0.8 (0.35)	+0.5 (0.35)	--	--	-1.7 (0.40)	-1.8 (0.40)
	Additional line LE	-1.4 (0.11)	-2.1 (0.11)	--	--	-4.0 (0.10)	-4.1 (0.10)

Table 5. Comparison of the chemical shifts of binding energies of peaks in the XPS spectrum of SbSI ethanogel prepared sonochemically with the data reported for SbSI and Sb_3I (LE – low energy line; HE – high energy line; [a)]- (Nowak et al., 2009e); [b)]- (Ikemoto, 1981); [c)]- (Grigas et al., 2004); [d)]- (Grigas et al., 2007); [e)]- (Grigas & Talik, 2003); [f)]- (Nowak et al., 2010d); In parenthesis there are relative intensities (in comparison with the intensity of the main line)).

The XPS measurements revealed the chemical shift in the SbSI ethanogel of Sb states of +(2.0÷2.1) eV to a higher binding energy, and S states of -3.2 eV and I states of -(0.1÷0.2) eV to a lower binding energy (Table 4 and 5). These shifts suggest a charge transfer from Sb to S and I - more to S than to I. One can see that probably in surface layer of SbSI nanowire the Sb atom transfers more electrons than the Sb in bulk SbSI crystals (Table 5). As a result, the surface layer of SbSI nanowire crystal is more ionic one while in SbSI crystals are less ionic. It means that the bonding environments of the atoms at surfaces of the sonochemically prepared SbSI nanowires and at SbSI single crystals grown from a vapour phase are different.

Taking into account that the splitting of spin-orbit doublets into different components may be induced by the contributions of atoms with different ion charges, the main Gaussian components of each peak in XPS spectra of surface layer of SbSI nanowires (see Fig. 10 and Table 5) were assigned (Nowak et al., 2009e) to the antimony subiodide. Due to relatively good coincidence between chemical shifts observed for the additional lines in XPS of SbSI ethanogel and the data reported for SbSI single crystals (see Table 5), these contributions were recognized as appropriate ones of SbSI (Nowak et al., 2009e).

Element		Sb	S	I	C
Concentration determined in the XPS investigations (at. %)	all detected elements	38	25	28	9
	components without C	42	27	31	--
	components without SbSI and C	15	--	4	--
	components in hypothetical Sb_xI_y	79	--	21	--
Concentration determined in the EDX investigations (at. %)	all elements	36	30	34	--
	components without SbSI	6	--	4	--
	components in hypothetical Sb_xI_y	60	--	40	--

Table 6. Atomic concentration of components of the sonochemically prepared SbSI ethanogel determined by XPS and EDX (after (Nowak et al., 2008e)

The XPS measured (Nowak et al. 2009e) atomic concentrations of Sb, S, I and C in SbSI ethanogel are compared in Table 6 with the results of energy dispersive X-ray (EDX) analysis averaged over the investigated sample (Nowak et al., 2008). Due to the large excess of Sb and the smaller excess of I detected by XPS chemical analysis (Table 6), probably a separate phase of Sb and I is present on the surface of the SbSI. It is improbable that the excess Sb and/or I are present within the ordered nanowires, since the mentioned above interplanar spacing corresponds to stoichiometric bulk SbSI. In fact, the sonochemically produced crystalline SbSI-type nanowires are completely surrounded by fuzzy shells (see e.g. Fig. 8). The growth of these nanowires from elements (Sb, I, and S or Se) in ethanol needs transport of the components to the surface of the growing crystal structure. It is very probable that the transported components are composed of small clusters. Before they are built into the crystal structure of the nanowire, they should be adsorbed on its surface. The composition of such surface layer may be different than the bulk of the SbSI-type nanowires,

due to different solubilities, transport parameters and chemical activity of Sb, S and I (as well as their ions and hypothetical compounds) in ethanol. It gives the possible explanation of the difference between the XPS measured concentration of the essential components of the SbSI nanowires (Table 6) and their concentrations in an ideal SbSI crystal (i.e. the 33.33 at % of Sb, S and I).

From the XPS data it was concluded (Nowak et al., 2009e) that the surface layer of SbSI nanowires contains SbSI (the sulfur is mainly inside it) and some additional material - the hypothetical antimony subiodide (Sb_xI_y) with the atomic ratio of Sb:I of about 79:21. However, it should be noticed that this composition is comparable with composition of the sonochemically prepared Sb_3I (Nowak et al., 2010d). Comparison of the XPS data presented in Tables 4 and 5 proves that the last compound can exist in surface layer of sonochemically prepared SbSI nanowires. Ratios of the hypothetical Sb_xI_y to SbSI components determined by XPS and EDX investigations are about 53 % and 20 %, respectively (Table 6). However, one should have in mind that the total XPS and EDX signals contain different contributions from the surface layer and bulk of the investigated material. Essentially, the XPS gives better information on the surface properties than the EDX technique.

The EDX (Fig. 11b) measured atomic concentrations of 0.46:0.21:0.33 of Sb, S and I in SbSI grown in CNT (Nowak et al., 2008c) are very similar to the concentrations determined by XPS in sonochemically prepared SbSI ethanogel (Table 6). It seems that the additional antimony subiodide phase exists between the CNT walls and the grown inside SbSI. Due to the large excess of Sb and the deficit of Se detected by EDX (the atomic ratio of 0.41:0.26:0.33 for Sb, Se and I (Fig. 11a)), probably the same separate phase of Sb and I is present and presumably it is adsorbed on the surface of the SbSeI nanowires (Nowak et al., 2009b). It should be underlined that the EDX analysis performed on SbSI methanogel with larger lateral dimensions of nanowires and about twice thinner fuzzy shells confirmed an elemental atomic ratio of 0.35:0.34:0.31 for Sb, S and I averaged over the sample (Starczewska et al. 2009).

The EDX analysis (Fig. 12) performed on individual nanowire of $SbS_{0.75}Se_{0.25}I$ with very thin fuzzy shell confirmed an elemental atomic ratio of 0.33:0.28:0.07:0.32 for Sb, S, Se and I (Nowak et al., 2010b). The characteristic peaks of Cu in Fig. 12 have their origin in sample support.

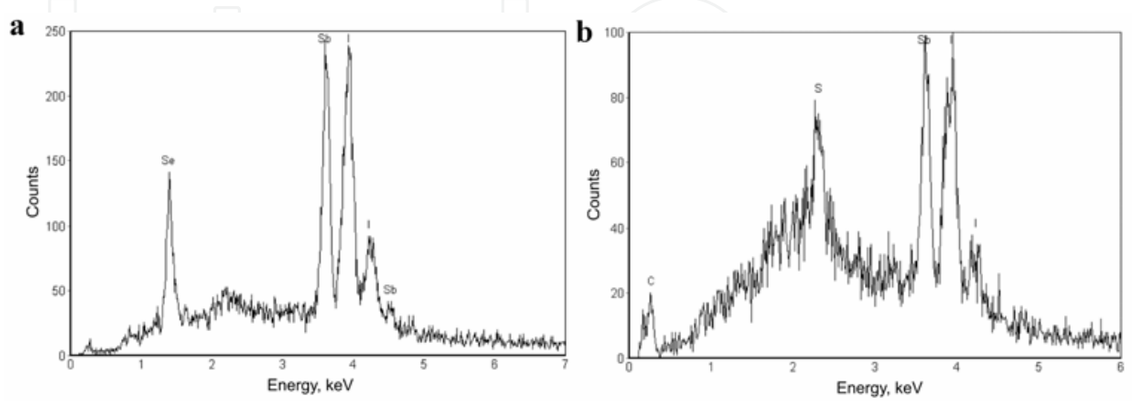


Fig. 11. The EDX spectra of SbSeI xerogel sonochemically prepared in ethanol (a after (Nowak et al., 2009b)) and of dried multiwalled CNTs filled sonically in methanol with SbSI (b after (Nowak et al., 2009c))

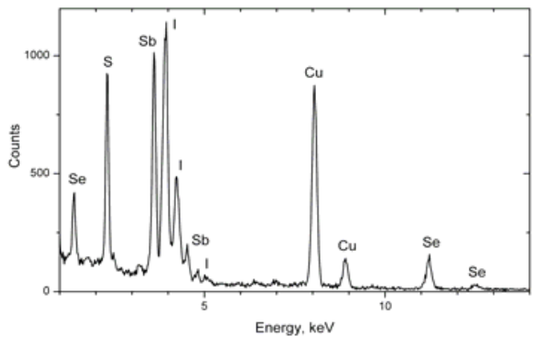


Fig. 12. The EDX spectrum of an individual nanowire from sonochemically prepared $SbS_{0.75}Se_{0.25}I$ (after (Nowak et al., 2010b)

5. Optical properties of photoferroelectric nanowires

5.1 Diffuse reflectance and optical energy gap of SbSI-type nanowires

The spectrum of diffuse reflectance signal R_d (the ratio of intensities of radiation reflected in diffuse manner from the sample and from the known standard) of SbSI xerogel is presented in Fig. 13. Usually the R_d values are converted to the Kubelka-Munk function (Philips-Invernizzi et al., 2001) proportional to the absorption coefficient of light (α)

$$F_{K-M}(R_d) = \frac{(1-R_d)^2}{2R_d} \sim \alpha \tag{7}$$

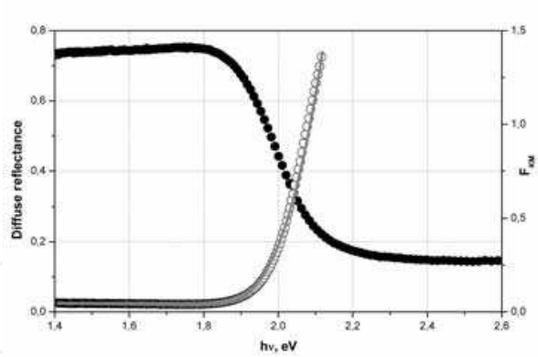


Fig. 13. Spectra of the diffuse reflectance coefficient (●) and the calculated F_{K-M} function (○) of SbSI nanowires sonochemically prepared in ethanol. Solid curve represents the fitted theoretical dependence (values of the fitted parameters are given in Table 7) (after (Nowak et al., 2009a))

It has been proved (Nowak et al., 2009a) that the best method of determining energy band gap (E_g) is based on simultaneous fitting of many mechanisms of absorption to the spectral dependence of F_{K-M} function evaluated from the diffuse reflectance spectroscopy (DRS). This method allows determining not only E_g and the main mechanism of absorption but also gives information on the coexisting phenomena. Therefore, the spectral dependence of the F_{K-M} function should be fitted by minimization of the following least square function

$$\chi^2 = \sum_{i=1}^{n} [(F_{KM}(h\nu_i) - B\sum_j \alpha_j(h\nu_i)]^2 \quad (8)$$

where i represents photons of different energy, α_j describes various mechanisms of light absorption, B is the proportionality factor.

Figure 13 presents the spectrum of F_{KM} of the investigated SbSI nanowires and the least square fitted theoretical dependence appropriate for the sum of indirect forbidden absorption without excitons and phonon statistics (α_1), Urbach ruled absorption (α_2), and constant absorption term (α_3) (see Refs. in (Nowak et al., 2009a)):

$$\alpha_1 = A_{60}(h\nu - E_{gIf})^3 \qquad \text{for } h\nu > E_{gIf} \quad (9)$$

$$\alpha_2 = A_U \exp\left[\frac{h\nu}{E_U}\right] \quad (10)$$

$$\alpha_3 = A_0 \quad (11)$$

where E_{gIf} represents the indirect forbidden energy gap, E_U is the Urbach energy, A_{60} is constant parameter proportional to the probability of photon absorption due to fundamental indirect forbidden transition in the investigated SbSI nanowires, and A_U is constant parameter proportional to the probability of absorption of photons due to Urbach transitions. The constant absorption term A_0 is an attenuation coefficient that is considered as the sum of the scattering and/or absorption independent of hν near the absorption edge.

	Values obtained for				
Fitted parameters	SbSI nanowires[a)]	SbSI nanowires[b)]	SbSI nanowires[c)]	CNTs filled with SbSI[d)]	SbSI crystals[b)]
E_{gIf}, eV	1.81(1)	1.829(27)	1.854(3)	1.871(1)	1.790(31)
$B{\cdot}A_{60}$, $1/(eV^3m)$	45.28(24)	54.83(14)	157(1)	95.6(7)	35.20(27)
A_{125} , 10^{12} m^{-2}		--	--	8.24(1)	
A_0, m^{-1}	0.0488(1)	0.0321(13)	0.0213(1)	2.702(3)	0.0141(17)
E_U, eV	0.571(7)	0.1031(16)	0.1470(20)	--	0.1027(43)
$B{\cdot}A_U$, 10^{-9} m^{-1}	$279(6){\cdot}10^3$	0.3570(19)	84.4(3)	--	0.2523(67)

Table 7. Comparison of the values of SbSI ethanogel parameters ([a)]- (Nowak et al., 2009a); [b)]- (Nowak et al., 2008)), SbSI methanogel ([c)]- (Starczewska et al., 2009)), multiwalled CNTs filled with SbSI in methanol ([d)]- (Nowak et al., 2009c)), and powdered SbSI single crystals ([b)]) that were determined from the fitting of the spectrum of Kubelka-Munk function evaluated from the measured diffuse reflectance

The fitting presented in Fig. 13 is rather good. Values of the fitted parameters (Table 7) are well compared with other literature data. The value E_{gIf}=1.81(1) eV of the indirect forbidden energy band gap of SbSI nanowires is close to the value evaluated for powdered SbSI single crystals (E_{gIf}=1.79(31) eV (Nowak et al., 2008)). It is also comparable to the bulk values of band gap of SbSI: 1.82 eV at 301 K (Fridkin, 1980) for the light polarized in [001] direction,

i.e. in the direction of growth of SbSI nanowires. The E_g for light polarized in perpendicular direction is slightly bigger (Fridkin, 1980). The greater Urbach absorption in the case of SbSI produced in methanol (Table 7) is probable due to the larger amount of crystal defects and additional electron states in its energy gap or due to the coexistence of different phases.
Figure 14a shows the large (about 100 nm) shift to the longer wavelengths of the absorption edge with the increase of Se content in $SbS_{1-x}Se_xI$ nanowires sonochemically prepared in ethanol. Figure 14b presents the rather good fitting of the F_{K-M} spectra with theoretical dependences appropriate for the sum of indirect forbidden absorption without excitons and phonon statistics (9), Urbach ruled absorption (10) and constant absorption term (11). It should be underlined that the same mechanisms of light absorption exist in $SbS_{1-x}Se_xI$ nanowires for any molar composition ($0 \le x \le 1$). The values of indirect forbidden energy gaps determined for the sonochemically produced $SbS_{1-x}Se_xI$ xerogel can be well fitted (Fig. 15) with a linear function of the molar composition

$$E_{gIf}(x) = A + B \cdot x \tag{12}$$

where A=1,852(5) eV, B=-0,210(9) eV (Nowak et al., 2010b). Figure 15 presents also comparison of the obtained results with the literature data for bulk $SbS_{1-x}Se_xI$.

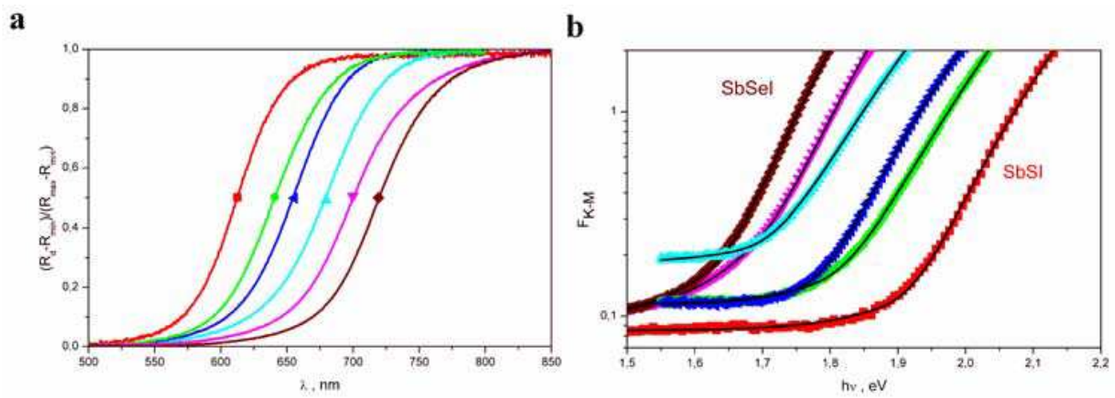


Fig. 14. Comparison of the diffuse reflectance spectra (A) and the calculated spectra of Kubelka-Munk functions (B) of $SbS_{1-x}Se_xI$ nanowires with different molar compositions (■- SbSI, ●- $SbS_{0.8}Se_{0.2}I$, ◀- $SbS_{0.6}Se_{0.4}I$, ▲-$SbS_{0.4}Se_{0.6}I$, ▼- $SbS_{0.2}Se_{0.8}I$, ♦- SbSeI; R_{min} , R_{max} – minimum and maximum value of the coefficient of diffuse reflectance in the investigated spectra range). Solid curves in Fig. 14B represent the fitted theoretical dependences for the sum of indirect forbidden absorption without excitons and phonon statistics, Urbach ruled absorption, and constant absorption term (values of the fitted energy gaps are given in Fig. 15) (after (Nowak et al., 2010b))

In Fig. 16a the diffuse reflectance spectrum of multiwalled carbon nanotubes (CNTs) filled sonochemically in methanol with SbSI is compared with the spectrum registered for hollow CNTs in methanol. In the first case one can see the characteristic, for semiconducting materials, edge of fundamental absorption around 615 nm. However, the diffuse reflectance decreases also with increasing wavelengths (Fig. 16a), probable due to the large amount of free carriers absorbing light. The best fitting of the spectrum of calculated F_{K-M} function was obtained for the sum of indirect forbidden absorption without excitons and phonon statistics (9), constant absorption term (11) and free carrier absorption (α_4) (Nowak et al., 2009c)

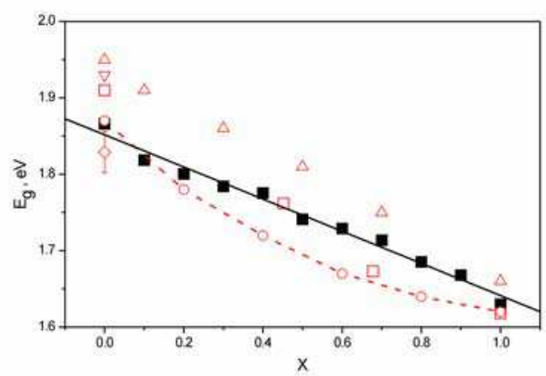


Fig. 15. Energy gap of $SbS_{1-x}Se_xI$ vs. molar composition (■- for nanowires (Nowak et al., 2010b); □- (Belayev et al., 1968); ○-(Park et al., 1990); △,▽- for plane polarized light with electric field perpendicular and parallel to the c-axis, respectively (Turjanica et al., 1969), ◇- for nanowires (Nowak et al., 2008); line represents the least square fitted linear dependence (12)) (after (Nowak et al., 2010b))

$$\alpha_4 = A_{125}\,\lambda^2 \tag{13}$$

where A_{125} is a constant parameter, and λ is the wavelength of radiation. The fitting presented in Fig. 16b is rather good. The determined values of parameters are given in Table 7. The nanocrystalline SbSI filling the CNTs is a semiconductor with little larger energy gap than the alone SbSI nanowires (Table 7). To test if this shift is due to the quantum size effect (Hui, 2000) the synthesis of SbSI in CNTs of smaller diameters is needed.

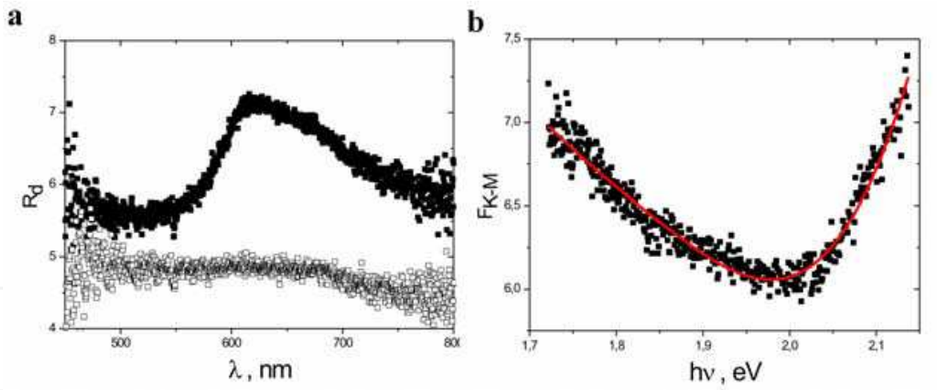


Fig. 16. (a) Comparison of the diffuse reflectance spectra of the multiwalled CNTs filled with SbSI (■) and of the empty multiwalled CNTs (□) in methanol. (b) Fitting of the spectrum of calculated F_{K-M} function of the multiwalled CNTs filled with SbSI. Solid curve represents the least square fitted theoretical dependence (values of the fitted parameters are given in Table 7) (after (Nowak et al., 2009c)

It is known (see e.g. (Eletskii, 2004)) that a metal atom intercalated inside the internal cavity of a CNT displays a tendency towards the transfer of some part of the valence electrons to the outer surface of the nanotube, where unoccupied electronic states exist. As a result of such a transfer there arises an additional mechanism of electrical conduction, related to the travel of an electron about those states in CNTs. The observed free carrier absorption of light

in the case of CNTs filled with SbSI is evoked by the CNTs material because it is absent in the case of alone SbSI nanowires (Table 7).

5.2 Temperature dependence of optical energy gap and spontaneous polarization

In Fig. 17 one can see the shift of fundamental absorption edge to longer wavelengths with increasing temperature of about 30 μm thick film of SbSI ethanogel.

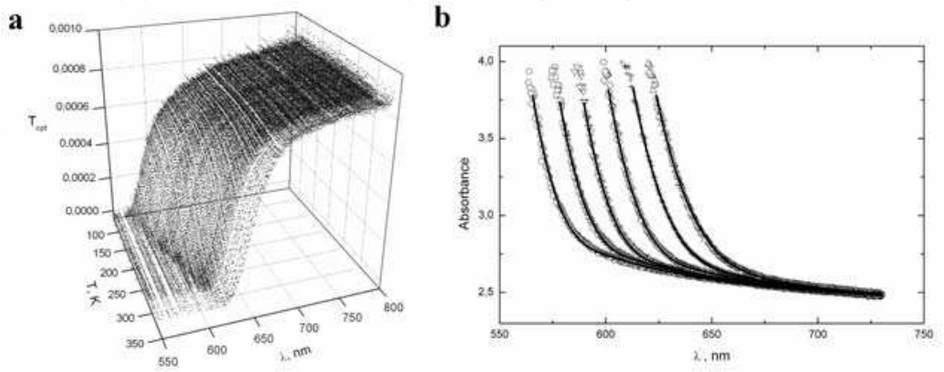


Fig. 17. (a) Influence of temperature on spectral characteristics of optical transmittance of a film of SbSI xerogel. (b) Typical spectra of absorbance of SbSI xerogel at different temperatures (○ - 80 K; □ – 150 K; ▽- 200.1 K; ◇- 250.1 K; +-296.8 K; △- 344.1 K; p=1.33 Pa). Solid curves represent the fitted theoretical dependences (values of the fitted parameters are given in Table 8) (after (Nowak & Szperlich, 2010))

T, K	Fitted parameters				
	E_{gIf}, eV	A_{60}, $1/(eV^3m)$	E_U, eV	A_U, 1/m	A_0, 1/m
80	2.066(5)	405(4)	0.2564(1)	$1.088(1)\cdot10^{-4}$	2.4011(6)
150	2.019(4)	423(3)	0.2329(1)	$5.051(5)\cdot10^{-5}$	2.4160(5)
200.1	1.976(3)	417(2)	0.2063(1)	$1.722(2)\cdot10^{-5}$	2.4258(4)
250.1	1.926(3)	369(2)	0.1709(1)	$2.627(3)\cdot10^{-6}$	2.4391(4)
296.8	1.879(3)	302(1)	0.1424(5)	$3.203(3)\cdot10^{-7}$	0.2448(4)
344.1	1.833(3)	220(1)	0.1195(4)	$3.076(3)\cdot10^{-8}$	0.2449(4)

Table 8. Influence of temperature on absorption parameters determined by fitting the absorbances spectra of SbSI xerogel (after (Nowak & Szperlich, 2010))

Figure 17b presents typical spectral dependences of SbSI xerogel absorbance at different temperatures fitted using numerical minimization of function (8). As in the DRS investigations of SbSI nanowires, the best results have been obtained for the sum of indirect forbidden absorption without excitons and phonon statistics (9), Urbach ruled absorption (10), and the constant absorption term (11). It should be underlined that these mechanisms of absorption of light do not change in the temperature range from 80 K to 344 K, i.e. in the ferroelectric and paraelectric phase of the SbSI. The fitting presented in Fig. 17b is rather good. Values of the fitted parameters are given in Table 8 and Figs. 18 and 19.

The optical energy gap of SbSI xerogel was determined for unpolarized light because the nanowires are variously directed in the investigated samples (see Fig. 8). For light with

electric field normal to the SbSI c-axis of bulk-size crystals the optical absorption edge shifts towards greater energies than for perpendicularly polarized light (Fig. 18a). Since, the determined E_{gIf} values of SbSI nanowires should be appropriate for the case of plane polarized illumination with electric field parallel to the SbSI c-axis.

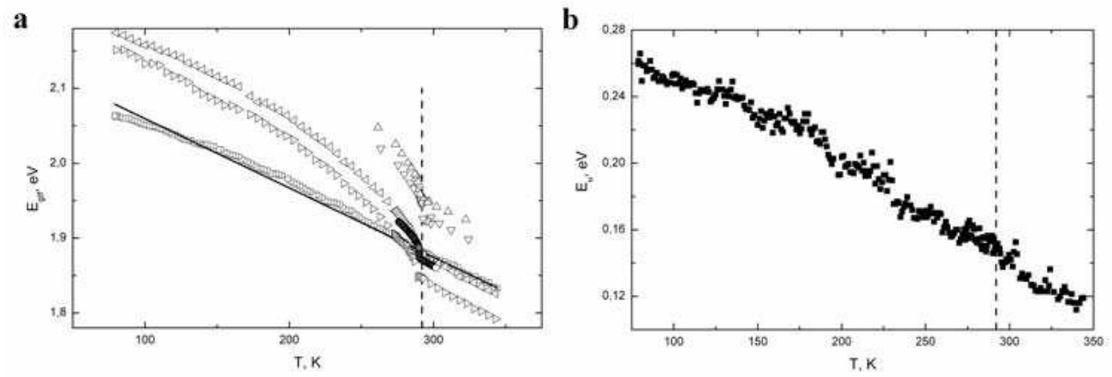


Fig. 18. Temperature dependences of (a) indirect forbidden energy gap (□) and (b) Urbach energy of SbSI nanowires and E_g of bulk SbSI crystals (△,▽- E_g defined by the izoabsorption energy corresponding α=150 cm^{-1} for plane polarized light with electric field normal ($\vec{E} \perp \vec{c}$) and parallel ($\vec{E} \parallel \vec{c}$) to ferroelectric c-axis, respectively (Ishikawa, 1980); ○ - izoabsorption energy corresponding α=150 cm^{-1} for $\vec{E} \perp \vec{c}$ (Audzijonis et al., 2008); ◁,▷- E_{gIf} for $\vec{E} \perp \vec{c}$ and $\vec{E} \parallel \vec{c}$, respectively (Nowak et al., 2003)). Solid line represents dependence (14) least square fitted to the experimental data in case of paraelectric phase (T_c=292 K < T < 344 K). Values of the fitted parameters are given in Table 9. The vertical dash lines show the Curie temperature (Szperlich et al., 2009) for SbSI nanowires (after (Nowak & Szperlich, 2010))

The mechanisms of optical absorption in SbSI xerogel evaluated using the presented absorbances and DRS data are the same (compare Tables 7 and 8). It should be underlined that the indirect forbidden absorption was reported for bulk-size SbSI by many investigators (see e.g. (Park et al., 1995)). Although, many other investigators described the optical properties of bulk-size SbSI using the Urbach absorption (see e.g. (Audzijonis et al., 2008)).
Comparison of the temperature dependence of the E_g of SbSI xerogel wit the data reported for bulk-size SbSI is difficult. Values of E_g reported for the same temperature are different (see e.g. Fig. 18a). Even the value of E_{gIf} of SbSI xerogel at 296.8 K (Table 8) is slightly bigger than the one derived from DRS at 297 K (Table 7). First of all, it can be a consequence of various methods used to evaluate the E_g (see e.g. (Nowak et al., 2009a)). Secondly, the E_g values depend not only on the actual phase of SbSI but also on the quality and history of the sample. For example, it was found that E_g is a function of spontaneous as well as induced electric polarizations of SbSI which in turn depend on the structure of ferroelectric domains and defects existing in crystal structure (see e.g. (Gerzanich et al., 1982)).
It is well known that the ferroelectric phase $Pma2_1$ disappears in SbSI crystals near room temperature (see chapter 4). The $E_{gIf}(T)$ dependences of SbSI xerogel (Szperlich et al., 2009) were least square fitted below and above T_c=292 K using the linear formula

$$E_{gIf}(T) = E_{g0} + \beta T \,. \tag{14}$$

Values of the determined parameters E_{g0} and $\beta=(dE_g/dT)_p$ are given in Table 9. The slope of $E_{gIf}(T)$ in the paraelectric phase of SbSI xerogel is in good conformity with data reported for bulk-size SbSI (compare Table 9 with the data cited in (Nowak & Szperlich, 2010)). The slope of $E_{gIf}(T)$ in the ferroelectric phase of SbSI xerogel is smaller than most of the slopes reported for bulk-size SbSI (see Fig. 18a and compare Table 9 with the data cited in (Nowak & Szperlich, 2010)). Only the $(dE_g/dT)_p$ reported in (Zeinally et al., 1974) for unpolarized illumination is quite comparable with the value determined for ferroelectric SbSI xerogel.

Fitted parameters	Ferroelectric phase (241 K < T < T_c=292 K)		Paraelectric phase (T_c=292 K < T < 344 K)	
	cooling	heating	cooling	heating
E_{g0} , eV	2.195(3)	2.189(4)	2.152(4)	2.152(5)
$(dE_g/dT)_p$, 10^{-4} eV/K	-10.8(1)	-10.5(2)	-9.3(1)	-9.2(2)

Table 9. Values of the determined parameters E_{g0} and $(dE_g/dT)_p$ of the linear temperature dependence (14) of E_{gIf} of SbSI xerogel (after (Nowak & Szperlich, 2010))

There is no discontinuity of the forbidden energy gap of SbSI xerogel larger than ΔE_{gIf}=0.0015 eV at T_c (Figs. 18a). Only the jump of $(dE_g/dT)_p$ in Curie point (Table 9) was observed. According to (Fridkin, 1966), it suggests that the ferroelectric phase transition in SbSI nanowires has the properties of the second-order phase transition. Unfortunately, there is very confused situation concerning the type of ferroelectric phase transition in bulk SbSI. Some authors have suggested that it is a first-order transition having features relevant to a second-order one. However, many other investigators have concluded that this transition is a first-order one (see Refs. in (Nowak & Szperlich, 2010)).

The Urbach energy (Fig. 18b) as well as the probability of Urbach absorption of photons (Fig. 19b) in SbSI xerogel increase with decreasing the temperature. According to (Cody et al., 1981), it should be due to the increase of disorder in the investigated material. Additional investigations are necessary to obtain the information about the possible disorder and the domain structure of the nanowires forming SbSI xerogel.

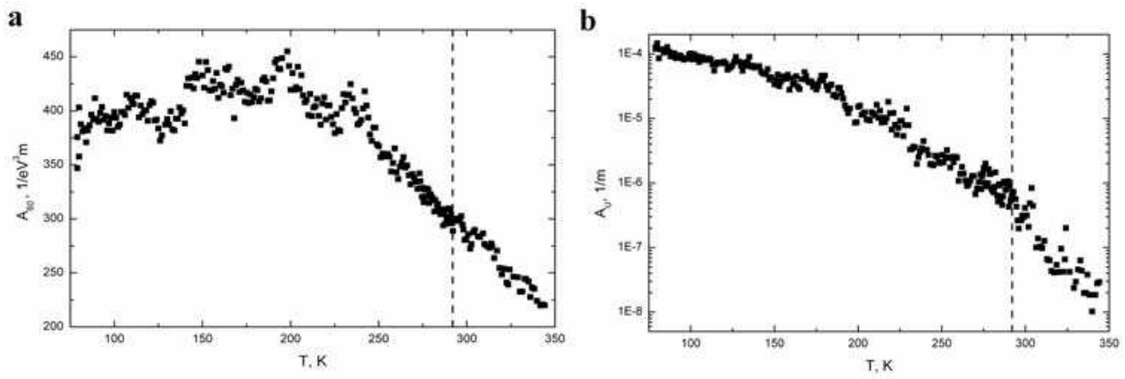


Fig. 19. Temperature dependences of the probability of absorption of photons due to fundamental, indirect, forbidden transitions (a) and of the probability of Urbach absorption of photons (b) in SbSI nanowires. The vertical dash lines show the temperature of the ferroelectric transition in SbSI nanowires (after (Nowak & Szperlich, 2010))

It is interesting that the temperature dependence of the probability of photon absorption due to fundamental, indirect forbidden transition in SbSI nanowires (Fig. 19a) shows two different slops below and above 240 K. A low temperature phase transition at ~233 K in bulk-size SbSI was suggested from the analysis of some types of measurements (see e.g. (Fridkin, 1980) and Refs. in (Nowak & Szperlich, 2010)). These evidences, however, are not conclusive. There is no anomaly in the static dielectric constant, and thus if this transition is indeed real, it does not involve a soft IR optic mode (Samara, 1975). Hence, two explanations exist for the mechanism of low-temperature anomalies in SbSI (Gerzanich et al., 1982):

- the anomalies are the result of the second-order phase transition due to the mutual influence of the phonons and defects existing in the SbSI crystal chains,
- the low temperature anomalies in SbSI near 233 K are regarded as due to a process associated with the interaction between defects and domain walls.

The anomalies of spontaneous polarization at low temperature are absent in monodomain bulk SbSI crystals (Nakonechnyi et al., 1979). Since, in (Nowak & Szperlich, 2010) it was concluded that the SbSI nanowires are probably polydomain structures.

It should be noted that the change of the forbidden energy gap of SbSI nanowires near the Curie point (at 292 K) can be explained by the influence of spontaneous polarization (P_s) of this material (Nowak & Szperlich, 2010)

$$\Delta E_{gs} = E_f(T) - E_p(T) = \beta_3^X P_s^2(T) \tag{15}$$

where E_f is the energy gap determined in the ferroelectric phase, E_p is the value of energy gap evaluated by extrapolation of the straight line that fits $E_g(T)$ in the paraelectric region to the ferroelectric region, and β_3^X is the c-axis component of polarization potential independent of T for a free crystal. The values of β_3^X were determined using (15) and the experimentally determined temperature dependences of E_g and P_s of bulk SbSI in e.g. (Ishikawa, 1980; Žičkus et al., 1984).

Taking the value β_3^X =1.64 eVm^{4}C^2 as the appropriate for the case of plane polarized radiation with the electric field parallel to the ferroelectric c-axis of SbSI (Nowak & Szperlich, 2010), the pertinent parameters from Table 9, and using (15), the P_s values of the SbSI nanowires have been estimated for each temperature (Fig. 20). It should be underlined that the trend of temperature dependence of the spontaneous polarization near Curie temperature is the same in both cases of bulk-size SbSI and SbSI nanowires (see Fig. 20 and the figures published e.g. in (Ishikawa, 1980; Toyoda, 1986). Such calculated P_s of SbSI xerogel is about three times smaller than the one of SbSI single crystals (Fig. 20). Usually, the values of P_s reported for the bulk-size SbSI are in the range from 0.11 C/m^2 at 283 K (Popolitov et al., 1969) to 0.30 C/m^2 at 200 K (Žičkus et al., 1984). The spontaneous polarization 0.012 C/m^2 was reported for thin films of SbSI (Agasiev et al., 1973). The smaller P_s value in the SbSI xerogel is obviously caused by disordering in its structure. It can be explained by the fact that for minimizing electrostatic energy of the sample a polydomain configuration is more favorable than a monodomain particle (Kretschmer & Binder, 1979). Discussing these effects one should also remember that without the poling dc field (so, in the conditions of transmittance measurements of SbSI ethanogel (Nowak & Szperlich, 2010)) the polarization of bulk SbSI was smaller than 0.025 C/m^2 (Imai et al., 1966).

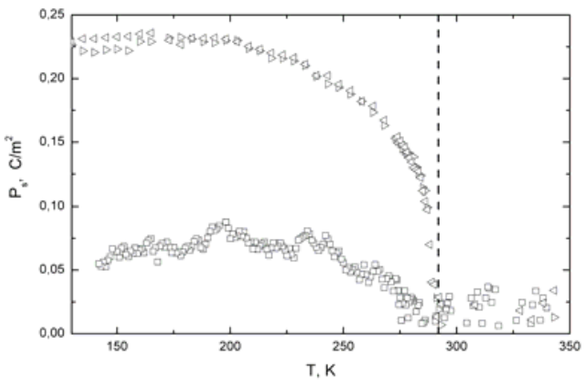


Fig. 20. Comparison of the temperature dependences of spontaneous polarization in SbSI nanowires (□) with data evaluated for bulk-size SbSI crystals (◁,▷- values calculated using data reported in (Nowak et al., 2003) for plane polarized light with electric field normal and parallel to ferroelectric c-axis, respectively). The vertical dash line shows the Curie temperature (Szperlich et al., 2009) of SbSI nanowires (after (Nowak & Szperlich, 2010))

5.3 Infrared absorbance of SbSI nanowires

The infrared (IR) absorbance of SbSI nanowires fabricated by sonochemical method in ethanol (Fig. 21a) is quite different from the one (Fig. 21c) of the SbSI methanogel. Both absorbance spectra have diffusive character due to the great porosity of the investigated samples. In the spectra range from 750 cm^{-1} to 4000 cm^{-1} the bulk crystalline SbSI practically does not show any absorbance lines (Fig. 21a). The IR absorbances of SbSI ethanogel and methanogel show some shifts of the observed bands in comparison with the IR spectra of ethanol (Fig. 21b) and methanol (Fig. 21c). The comparison of the IR absorbance spectra of as prepared SbSI ethanogel as well as SbSI methanogel and the samples heated to different temperatures is given in Fig. 22. The wavenumbers of main IR absorbance bands shown in Fig. 22 are presented in Table 10.

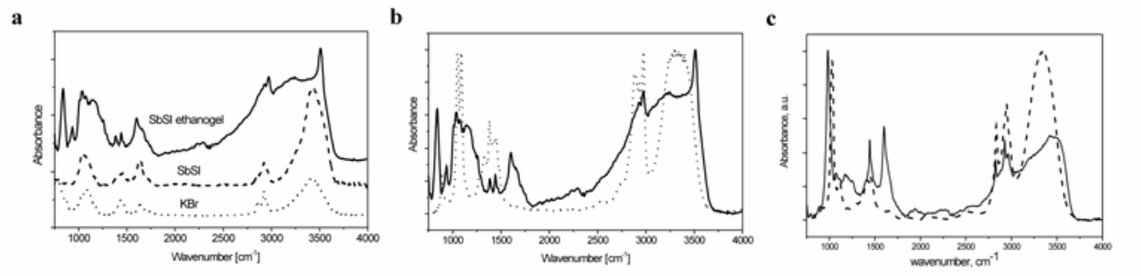


Fig. 21. Comparison of (a) IR absorbance spectra (without the background): — SbSI ethanogel as prepared, -- powdered SbSI single crystals embedded in KBr, ⋯ KBr alone (after (Starczewska et al., 2008)); (b) IR absorbance spectra of the SbSI ethanogel as prepared (—) and the spectra of ethanol (⋯) (after (Starczewska et al., 2008)); (c) Comparison of the IR absorbance spectra of the SbSI methanogel as prepared (—) with the spectra of methanol (--) (after (Starczewska et al., 2009)); All spectra were recorded at 300 K.

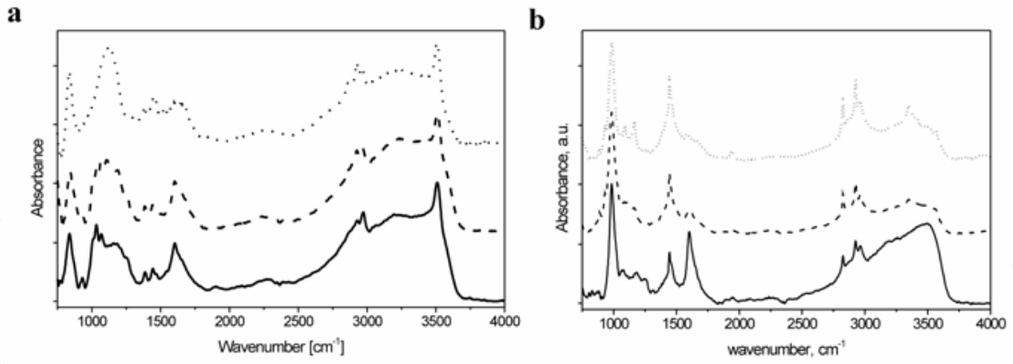


Fig. 22. Comparison of the IR absorbance spectra (without the background) of the SbSI ethanogel (a after (Starczewska et al., 2008)) and SbSI methanogel (a after (Starczewska et al., 2008)) heated to different temperatures: — as prepared, -- dried in vacuum (10^{-4} mbar) at T=353 K, ⋯ annealed in vacuum (10^{-4} mbar) at T=393 K. Drying and annealing were performed during 8 hours. All spectra were recorded at 300 K

Generally, in the case of SbSI nanowires sonochemically prepared in ethanol, the IR bands can be attributed to the vibrations inside the adsorbed C_2H_5OH molecules, C_2H_5O species, C_2H_4 molecules, OH groups, and H_2O molecules (Table 10). Probably these species are produced during the sonolysis. The postannealing eliminates the adsorbed water. However, Fig. 22a and Table 10 clearly illustrate the presence of OH, CH_2 and CH_3 groups on the surface of SbSI nanowires underwent high-temperature treatment in ultrahigh vacuum. In (Starczewska et al., 2008) it was shown that ethanol adsorbs dissociatively over SbSI nanowire surfaces via scission of the O–H bond to form two types of adsorbed ethoxide species (monodentate and bidentate). The reason for this behaviour is due to the phenomenon called the "proximity effect". Bonds tend to break when they are in relatively close proximity to the surface. The atomic arrangement has been considered almost consistent with the ionic model $Sb^{3+}S^{2-}I^{-1}$ (Kikuchi et al., 1967). The rather short distances between negative ions, on the other hand, suggest a partial covalency of the bond (Kikuchi et al., 1967). The adsorption of alcohols on ionic surfaces, like SbSI, is believed to involve dipole-induced dipole bonds. The dipole is strongest near the oxygen, and consequently the interaction with the surface is maximized if the oxygen of the alcohol is directed toward the surface. The formation of Sb-O bond is much easier from this configuration and thus O-H scission dominates. The adsorbed C_2H_5O may be further dehydrated to ethylene. The C_2H_4 is absorbed on the SbSI nanowire surface, too. Summarizing, one observes the ethanol dehydration over the surface of SbSI nanowires. In samples of gas desorbed from sonochemically prepared SbSI ethanogel and heated at temperature range 368 K to 373 K the ethanol and ethylene were detected using gas chromatographs (Starczewska et al., 2008).
Dehydration of alcohols is a characteristic reaction on acidic sites, i.e. Brönsted and Lewis sites, of transition metal oxides. Thus, C_2H_4 formation indicates the presence of higher acidic sites on the SbSI nanowires. Accordingly, S^{-2} or I^{-1} can act as donor site, whereas surface coordinatively unsaturated Sb^{3+} can act as electron acceptor (Starczewska et al., 2008).
It was mentioned in (Nowak et al., 2009d) that the ultrahigh vacuum conditions (10^{-8} Pa) and/or the used Al K_α monochromatic radiation (with 1486.6 eV energy) could affect desorption or photodesorption of ethanol, ethoxide species, ethylene and water from the surface of sonochemically fabricated SbSI nanowires. The XPS data (Nowak et al., 2009d) revealed no such species, at least within the detection limit of the analysis.

Wavenumbers, cm^{-1}			Mode description after	Wavenumbers, cm^{-1}			Mode description after
Methanogel of SbSI				Ethanogel of SbSI			
as prepared	dried	annealed		as prepared	dried	annealed	
				837	842	837	$\rho(CH_2)$ in C_2H_4
885	888	885	$\rho(CH_3)$ in CH_3I				
	930	929	γ(CO)				
				936	933	926	$\omega(CH_2)$ in C_2H_4
983	984	984	ν(CO)	1037	1029		ν(CO)
				1074	1064	1072	
				1105	1108	1112	
1075	1082	1091	$\rho_{ip}(CH_3)$				
1170	1162	1165	$\rho_{ip}(CH_3)$	1143	1148	1146	$\rho_{ip}(CH_3)$
				1255	1244	1269	δ(OH) or $\tau(CH_2)$
				1384	1384	1384	$\delta_s(CH_3)$
1444	1444	1443	$\delta_s(CH_3)$ or $\delta_{as}(CH_3)$	1441	1442	1447	$\delta(CH_2)$ in C_2H_4 or $\delta_{as}(CH_3)$
1601	1603		$\delta(H_2O)$	1602	1602		$\delta(H_2O)$
2825	2825	2825	$\nu_s(CH_3)$				
		2857	$\nu_{as}(CH_3)$		2853	2855	$\nu_s(CH_2)$ and $\nu_s(CH_3)$
2925	2925	2925	$\nu_{as}(CH_3)$ or $2\delta_{as}(CH_3)$	2928	2925	2925	$\nu_{as}(CH_3)$ or $\nu_{as}(CH_2)$
2962	2962	2961	$\nu_{as}(CH_3)$	2972	2967	2963	$\nu_{as}(CH_3)$
3419	3349	3347	ν(OH) in associated -OH; broad absorption band	3244	3234	3197	ν(OH) in associated -OH;broad absorption band
		3563	ν(OH) non-bounded	3510	3510	3508	ν(OH) non-bounded

Table 10. IR peak positions of the SbSI methanogel (Starczewska et al., 2009) and ethanogel (Starczewska et al., 2008) prepared in different conditions: as prepared, dried at 353 K in vacuum (10^{-4} mbar), annealed at 393 K in vacuum (10^{-4} mbar)

In the case of SbSI nanowires sonochemically prepared in methanol the IR bands (Fig. 22 and Table 10) can be attributed to the vibrations inside the adsorbed CH_3OH molecules, CH_3O species, dimethyl ether molecules, OH groups, and H_2O molecules. Probably these species are produced during the sonolysis. In (Starczewska et al., 2009) it was shown that

methanol adsorbs dissociatively over SbSI nanowire surfaces via scission of the O–H bond as in the case of ethanol. Such scission can form different types of adsorbed methoxide species: the monodentate and bidentate. The reason for this behaviour is the mentioned above "proximity effect". Hence, the surfaces of SbSI nanowires prepared sonically in methanol are covered with methoxide species and dimethyl ether (Starczewska et al., 2009).
It should be underlined that in contrary to the OH groups strongly absorbed on surfaces of SbSI ethanogel (see Fig. 22a), these groups are absent in the case of SbSI methanogel nanowires ensemble that underwent high-temperature treatment in ultrahigh vacuum (Fig. 22b). Because molecular adsorbates can compensate the surface polarization charges, providing a mechanism for reducing the depolarization fields, the electric properties of SbSI methanogel should be different from the properties of SbSI ethanogel. Additionally, in the case of SbSI ethanogel the adsorbed C_2H_5OH molecules were reported (Starczewska et al., 2008). Surprisingly, the whole molecules of CH_3OH were not adsorbed on the surfaces of SbSI nanowires or the amount of them was very small (Starczewska et al., 2009). Hence, the methanol decomposes more effectively than ethanol during the sonification or due to the adsorption process on SbSI nanowires.

6. Electrical and photoelectrical properties of photoferroelectric nanowires

6.1 Type of majority electric carriers in SbSI nanowires

In (Nowak et al., 2009d) the XPS was used to investigate the valence band (VB) in the sonochemically prepared SbSI nanowires at room temperature under ultrahigh vacuum conditions ($p=10^{-8}$ Pa). In the XPS spectrum of the VB region of the SbSI nanowires there are two main bands (Fig. 23). The lower binding energy band is over four times larger than the higher binding energy band. The valley between these bands is very deep. The overall shape of this structure is well compared to the VB in bulk SbSI single crystals and corresponds well to the calculated density of states in VB (Ikemoto, 1981; Grigas et al., 2007). According to the theoretical calculations the lower binding energy is the p-band and the higher binding energy band is s-band in VB. The experimental XPS of the valence band is the integral picture of all electronic states in the VB.
Since the optical energy gap of the SbSI ethanogel equals $E_{gIf}=1.81(1)$ eV (Table 7) and the VB determined in XPS measurements is located about 0.5 eV from the Fermi level (Fig. 23), the surface layer of sonochemically prepared SbSI nanowires is of p-type. It is dissimilar to

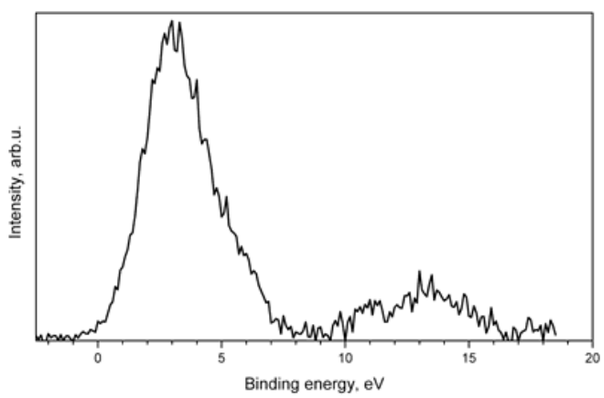


Fig. 23. XPS of the valence band of SbSI ethanogel (after (Nowak et al., 2009d)).

the n-type bulk SbSI single crystals that had VB separated by gaps of 1.8 eV and 2.3 eV from the Fermi level at temperatures 330 K and 215 K, respectively (Grigas et al., 2007). However, in XPS measurements of powdered SbSI crystals (Ikemoto, 1981), the VB was pinned to the Fermi level as should be in the case of p-type material. As to the nature of the conductive carriers in p-type SbSI (so, also in the sonochemically prepared SbSI ethanogel), it was proposed that the iodine vacancies in the SbSI lattice play the role of acceptors (Irie, 1973), or that some of the S^{2-} ions that replace the I^{-} ions play the part of acceptors (Toyoda & Ishikava, 1970).

6.2 Electrical conductivity of SbSI nanowires

Figure 24 shows the electric current response on the switch on of the dc bias voltage applied to the sonochemically produced SbSI ethanogel. The characteristic decrease of the current with time was noted. The saturated current showed an ohmic behavior with applied field E from -16 kV/m to 16 kV/m (Szperlich et al., 2009). One should notice that when the bias voltage was switch off the current changed its direction and then the drop in the negative current was observed (Fig. 24).

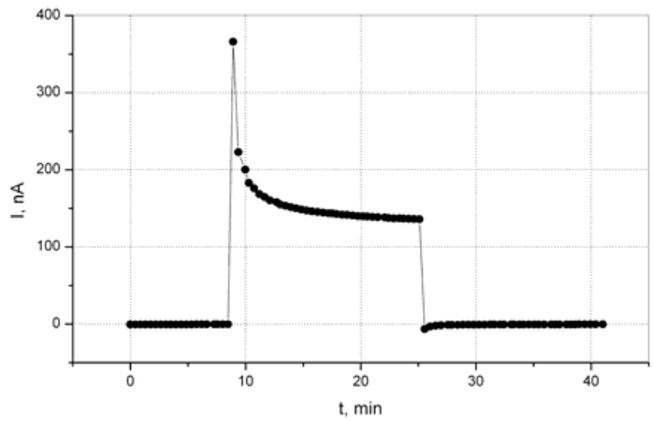


Fig. 24. Current response on the switch on and switch off of voltage applied to the sample of SbSI ethanogel (E=3300 V/m, T=295 K, p=1 atm, humidity 50 %) (after (Szperlich et al., 2009))

Unfortunately, even in the case of bulk SbSI single crystals the mechanism of electrical conduction is not fully understood. Investigations have shown that at contact of such ferroelectric with a metal a Schottky barrier is formed (Wemple et al., 1967). The surface states play a significant role in this case (Zhdan & Artobolevskaya, 1971). Their density may exceed 10^{14} $cm^{-2}eV^{-1}$ (Pipinys et al., 2004). In (Audzijonis et al., 2001) the electrical conductivity of bulk SbSI was explained employing Frenkel emission and a phonon-assisted tunneling. It was also supposed that the field induced phonon-assisted tunneling mechanism may dominate the charge transport process in the bulk SbSI (Pipinys et al., 2004). It was found that the current in bulk SbSI could be limited by the residual polarization charge or by the emission current flowing from the injecting electrode (Kosman & Sleptsov, 1971). The complicated structure of the sonochemically prepared SbSI ethanogel needs a quite new theoretical description of the electric conductivity of this material.

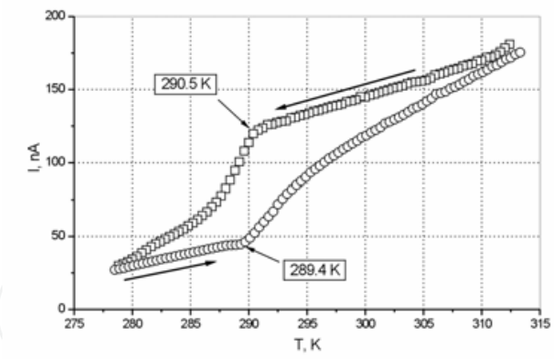


Fig. 25. Temperature dependence of electric current intensity in a sample of SbSI ethanogel upon heating (○) and cooling (□) (E=3300 V/m, p=1 atm, humidity 70 %) (after (Szperlich et al., 2009))

Temperature dependence of electric current in SbSI ethanogel proves its semiconductor properties (Fig. 25). The observed hysteresis of the electric current intensity in the heating-cooling cycle proves that this material is a ferroelectric with Curie temperature near 292 K. The difference between the electric current intensities upon cooling and heating attains maximum near the temperature 291.4 K that corresponds with the Curie temperature in bulk SbSI crystals (see chapter 6.3). The slope of the temperature dependence of electric current intensity changes radically near temperatures 289.4 K (under heating) and 290.5 K (under cooling), so near the Curie temperature (Fig. 25). This dependence was least squares fitted in the paraelectric and ferroelectric regions using the following relation

$$I = I_A \cdot \exp(-\frac{\Delta E_A}{k_B T}) \tag{16}$$

where ΔE_A represents activation energy, I_A is the proportionality factor, k_B and T have the obvious meanings. Table 11 summarizes the fitted values of ΔE_A for ferroelectric and paraelectric phases during heating and cooling of the sample.

Phase	Fitted activation energy, eV	
	cooling	heating
Ferroelectric	0.785(15)	0.346(6)
Paraelectric	0.105(9)	0.243(3)

Table 11. Comparison of the activation energies in temperature dependences of electric conductivity of SbSI ethanogel evaluated for ferroelectric and paraelectric phases during heating and cooling of the sample (after (Szperlich et al., 2009)

The thermal activation energy of the electric conductivity of bulk SbSI crystals was evaluated e.g. in (Popik & Betsa, 1988). The values of ΔE_A were different in the ferroelectric and paraelectric phases as it is in the case of sonochemically prepared SbSI ethanogel (Table 11). Unfortunately, the values of the reported ΔE_A are in very wide range (e.g. from 0.01 eV to 1.6 eV (Popik & Betsa, 1988)). It can be affected by very complicated structure of the electron levels in the energy gap of SbSI. Hence, it is difficult to present an interpretation of ΔE_A determined in the case of the sonochemically prepared SbSI ethanogel.

6.3 Dielectric properties of SbSI nanowires near the Curie point

The temperature dependences of dielectric constant and loss tangent of the sonochemically prepared SbSI ethanogel (Fig. 26) are typical for the temperature region near Curie point of ferroelectrics. The maximum of dielectric constant $\varepsilon=1.6\cdot10^4$ was observed for $T_c=292(1)$ K (Szperlich et al., 2009). The loss tangent of this material is relatively high and also shows its maximum (about 4.3) near T=292(1) K. Such a Currie temperature is characteristic for the single crystals of SbSI (Ishikawa, 1980; Toyoda, 1986).

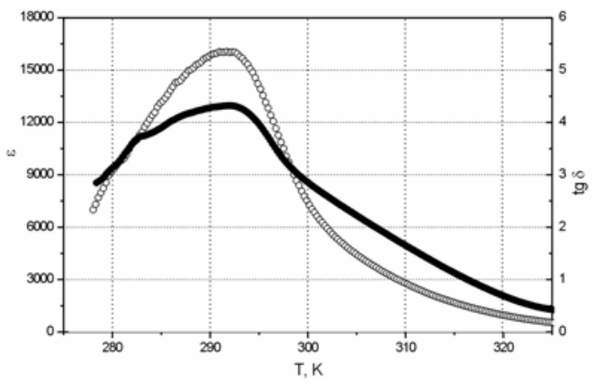


Fig. 26. Temperature dependence of dielectric constant (○) and loss tangent (●) of SbSI ethanogel at E=660 V/m and f=1 kHz (p=1 atm, humidity 70 %) (after (Szperlich et al., 2009))

The determined value of dielectric constant of the sonochemically prepared SbSI ethanogel is lower than the peak dielectric constant $\varepsilon=6.2\cdot10^4$ measured along the polar axis of the best SbSI crystals at $T_c=291$ K (Ishikawa et al., 1984). However, it should be noted that the peak dielectric constant measured in the case of SbSI ethanogel is higher than values reported for the best thin films of SbSI ($\varepsilon=5.2\cdot10^3$ at $T_c=292.3$ K for the pulsed laser deposited and annealed SbSI 4 μm films (Kotru et al., 2000)). One should remember that SbSI is a highly anisotropic material and the permittivity of SbSI single crystal of the polar direction is about 2000 larger than that of the perpendicular direction (Merz & Nitsche, 1964). The investigated SbSI ethanogel has disordered nanowires and very large porosity (see chapter 4), so the determined averaged value of its dielectric constant does not represent the exact value for an individual SbSI nanowire.

The loss tangent of the sonochemically prepared SbSI ethanogel is much higher than the values reported for bulk crystals and thin films of SbSI. Probably, it is due to the complicated structure of the investigated samples of SbSI ethanogel. However, it should be underlined that the great value of the loss tangent sometimes can be a positive feature of ferroelectrics, for example in TANDEL (Rittenmyer et al., 1988).

6.4 Photoconductivity of SbSI nanowires

In (Nowak et al., 2010a) about 5 μm thick samples of as synthesized sonochemically SbSI ethanogel were deposited upon interdigitated finger electrodes on alumina substrates with heaters and temperature detectors. The ethanol was evaporated from them in air at 313 K and a so-called xerogel films were obtained (made up of single crystalline SbSI nanowires with diameters of about 10-50 nm and lengths reaching up to several micrometers). To normalize the photoconductive current of the SbSI ethanogel for constant illumination, the experimental results (Fig. 27) were least square fitted with semiempirical power equation

$$I_{PC}(h\nu,T) = A(h\nu,T)\, I_0^{\gamma(h\nu,T)} \tag{17}$$

where I_0 – incident light intensity, γ(hν,T), A(hν,T) - coefficients which depend on photon energy and temperature. The values of power coefficients γ(hν,T) (Fig. 28), evaluated using this fitting, are smaller than one and indicate the nonlinear recombination of carriers in SbSI nanowires with the increase of excess carrier concentration. Using the determined values of A(hν,T) and γ(hν,T), the spectral characteristics of I_{PC}(hν,T) were normalized for various constant light intensities (Fig. 27b). These characteristics are typical for the case of surface recombination of the excess carriers (Gärtner, 1957).

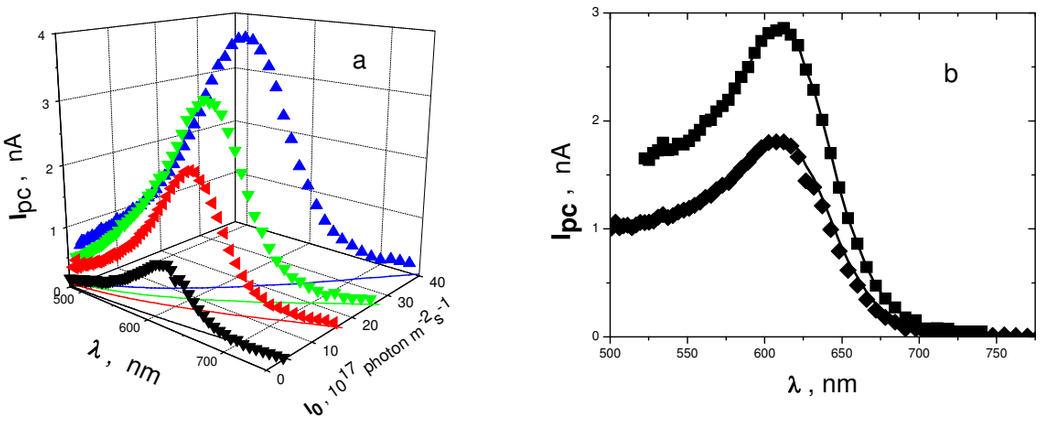


Fig. 27. (a) Experimental data of spectral dependences of photoconductive currents in SbSI ethanogel at 323.7 K (p=1.33 Pa). Solid curves show the spectral dependences of illumination intensities; (b) Normalized for different light intensities spectral characteristics of photoconductivity (◆- I_0=5·10^{17} photons m^{-2}s^{-1}; ■- I_0=10^{18} photons m^{-2}s^{-1}; T=323.7 K). Solid curves represent theoretical dependence (18) calculated for the values of the fitted β (Fig. 28b) as well as W, S_1 and S_2 (Fig. 29) (after (Nowak et al., 2010a))

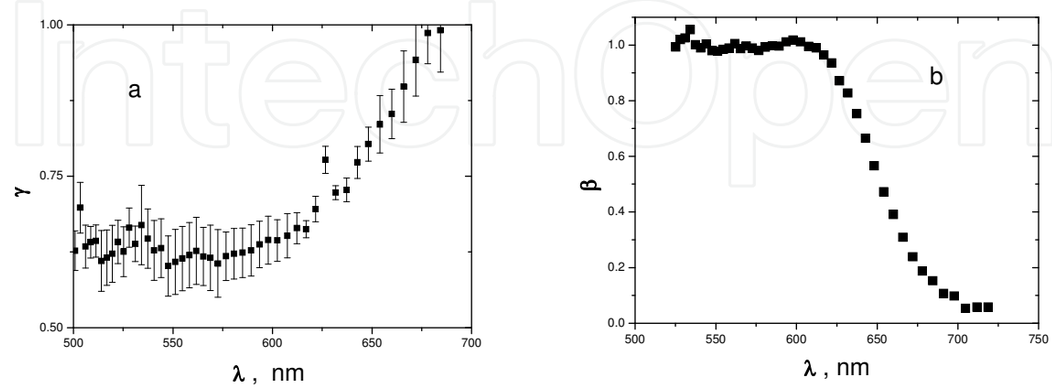


Fig. 28. Spectral dependences of (a) power coefficient from equation (17) least-squares fitted to the experimental data of photoconductivity of SbSI ethanogel and (b) the quantum efficiency coefficient for photogeneration of carriers (T=323.7 K) (after (Nowak et al., 2010a))

The change of recombination velocity with the increase of excess carrier concentration evokes the cumbersome theoretical description of nonlinear dependence of I_{PC} on the illumination intensity. However, in the first approximation of this problem, one can take into consideration different values of recombination parameters (i.e. ambipolar carrier diffusion length L, surface recombination velocities s_1 and s_2 at the front and back surfaces of the sample) for each intensity of illumination (Szałajko & Nowak, 2007). In such a case, the I_{PC} can be described by the theory presented in for example (Gärtner, 1957)

$$I_{PC} = A_{pc}(1-R_d)I_0\beta\frac{K}{W^2-K^2}\frac{1}{W}\left[\frac{(K-S)(W-S)\left(1-e^{-W}\right)e^{-K}+(K+S)(W+S)\left(1-e^{W}\right)}{(W+S)(W+S)e^{W}-(W-S)(W-S)e^{-W}}\right. \tag{18}$$

$$\left.-\frac{(K-S)(W+S)\left(1-e^{-W}\right)e^{-K}+(K+S)(W-S)\left(1-e^{-W}\right)}{(W+S)(W+S)e^{W}-(W-S)(W-S)e^{-W}}+\frac{W}{K}\left(1-e^{-K}\right)\right]$$

where $S=s_1w/D=s_2w/D$ is dimensionless surface recombination velocity on the front and back surfaces, $K=\alpha w$ is the dimensionless absorption coefficient, w the sample thickness, $W=w/L$ the dimensionless sample thickness, β the quantum efficiency coefficient for photogeneration of carriers, A_{pc} is a proportionality constant dependent on geometrical dimensions of the sample, the electron and hole mobilities, the ambipolar diffusion coefficient of carriers, the electric field strength, and elementary charge.

In (Nowak et al., 2010a) values of $\alpha(h\nu,T)$ and $R_d(h\nu,T)$ have been determined experimentally. The results are very similar to the presented in chapters 5.1 and 5.2. Normalized spectral dependences of photoconductivity (e.g. the presented in Fig. 27b) have been least-squares fitted using equation (18) for different light intensities. The fitting was performed for photon energies characteristic for intrinsic photogeneration, i.e. for quantum efficiency coefficient equal β=1. Then the real value of β has been evaluated (Fig. 28b) applying the method described in (Szałajko & Nowak, 2007). It allowed determining also the influence of illumination intensity on recombination parameters of carriers in SbSI nanowires (Fig. 29).

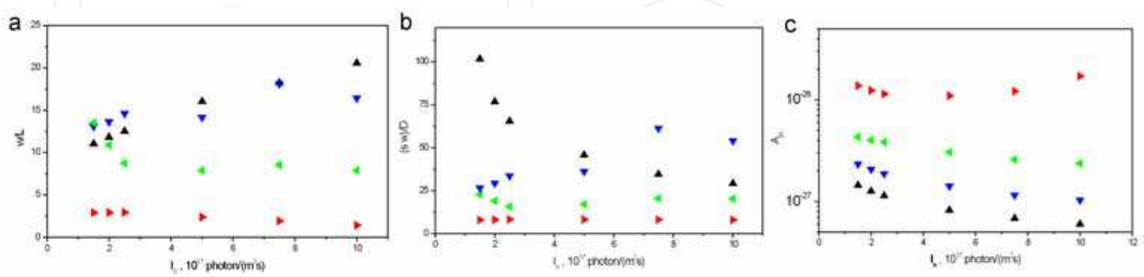


Fig. 29. Influence of illumination intensity on ambipolar diffusion length (a), surface recombination velocity (b), and A_{pc} factor (c) in aligned SbSI nanowires at different temperatures (▲- 263 K; ▼- 283 K; ◀- 303 K; ▶- 323 K; p=1.33 Pa) (after (Nowak et al., 2010a))

The nonlinear recombination of carriers in SbSI nanowires needs future investigations that should result in the determination of mechanism of the recombination as well as energetic

positions, concentrations and cross-sections of electron states in the energy gap of this material. Probably, a quite new model of photoconductivity in xerogels composed of nanowires is necessary.

7. Conclusions

The SbSI-type well crystallized nanowires, belonging to the class of photoferroelectrics, can be prepared using very simple sonochemical synthesis from elements at low temperature and ambient pressure. Such bottom-up technique is convenient, fast, mild, efficient (with a yield approaching 100 %), and an environmentally friendly route of production of nanowires with uniform shape and high crystallinity in a single step. It may be predicted that upscaling of this method will lead to large quantities of SbSI-type nanowires with uniform morphology and high purity. It seems that this approach can be extended to the preparation of some other ternary and quaternary nanomaterials formed from the group 15-16-17 elements. It should be remember that the physical properties of such quaternary compounds, formed as solid solutions, can be tailored with stoichiometric composition. It should be an advantage of using such material in different devices.

Up to now the polar solvents (ethanol and methanol) were used in the sonochemical synthesis of SbSI, SbSeI and $SbS_{1-x}Se_xI$ nanowires. Temperature of the synthesis was low but still higher than the ones of ferroelectric phase transitions of these materials. It should be interesting to investigate if the unpolar liquids (e.g. toluene) as well as temperature of sonolysis lower than the Curie temperature of the product (i.e. lower than 291 K for SbSI) can influence the rate of preparation of SbSI-type nanowires and the properties of the products. The growing of materials in ferroelectric state should be interesting at least for fundamental investigations on nanoscale ferroelectricity and on mechanisms of crystal growth. In contradistinction to all techniques used for growth of the bulk SbSI-type crystals, the sonochemistry makes such an approach rather easy and may be effective.

One of the features of the presented SbSI-type nanomaterials is that they are formed sonochemically as xerogels. The high surface-to-volume ratios associated with these nanostructures, possessing semiconducting as well as ferroelectric properties, make them very interesting for the sensing of important molecules or for using as electrodes. The catalytic properties of SbSI-type nanomaterials, e.g. suitable for alcohols decomposition, should be investigated. However, further studies on the cross-linking of SbSI-type nanowires in sonochemically prepared xerogels and on the role of the surface layers of these nanowires are needed to establish the xerogels more fracture-tough. Further studies on the electrophysical properties of the presented as well as the other ternary and quaternary SbSI-type nanomaterials are needed. Especially, the impedance spectroscopy should give information on the structure of the sonochemically prepared xerogels.

The presented sonochemical synthesis of nanophase SbSI in carbon nanotubes should be extended to the preparation of some other nanomaterials formed from the group 15-16-17 elements within CNTs. Such hybrid objects should be distinguished in their properties from both hollow nanotubes and the encapsulated substances, which permits one to purpose-tailor "nanowires" and "nanocables" with unique physical and chemical properties (Friedrichs et al., 2005). Special interest is in investigations on SbSI-type nanowires in single wall CNTs of smaller diameters. It may give an insight into quantum size effects in them.

This review summarizes all so far published results of investigations on SbSI-type photoferroelectric nanowires. One can see that the properties of the 1D SbSI-type materials

still remain little known. Meantime, nanowires of SbSI-type should provide promising materials for fundamental investigations on nanoscale ferroelectricity and piezoelectricity as well as materials for some applications. Probably, they may be useful in nanoscale nonvolatile memory applications. It is important because the Authors of (Yun et al., 2002) have suggested that ferroelectric $BaTiO_3$ nanowires may be used to fabricate nonvolatile memory devices with an integration density approaching 1 terabit/cm^2. Especially, investigations are necessary to obtain the information about the domain structure of the ferroelectric SbSI-type nanowires.

8. Acknowledgements

The author is indebted to Dr. P. Szperlich of the Silesian University of Technology, Katowice (Poland) for helpful discussions and his aid in preparing this paper. This review was partially supported by the MNiSzW (Poland) under contract No. N N507 1577 33.

9. References

Agasiev, A.A.; Zeinally, A.Kh. & Silvestrov, V.G. (1973). SbSI thin films with a ferroelectric phase transition, *Kristallografiya* 18 (1973) 1293-1294, ISSN: 0023-4761

Audzijonis, A.; Pipinys, P.; Lapeika, V. & Žaltauskas, A. (2001). Optical and electrical properties of SbSI single crystals, *Lith. J. Phys.* 41 (2001) 294-298, ISSN: 1648-8504

Audzijonis, A.; Žigas, L.; Žaltauskas, R.; Sereika, R. & Pauliukas, A. (2008). Origin of the Optical Anomalies Near the Ferroelectric Phase Transition in SbSI and SbSBr Crystals, *Ferroelectrics Lett. Sect.* 35 (2008) 51-61, ISSN: 0731-5171

Belayev, A. D.; Krivshich, V.V.; Micelyuk, E. G.; Slivka, V. Yu.; Turyanitza, I. D. & Chepur, D. V. (1968). Some electrical, optical and photoelectrical properties of $Sb_xBi_{1-x}SJ$ and $SbS_xSe_{1-x}J$ crystals, *Ukrainskii Fiz. Zhurnal* 13 (1968) 854-856, ISSN: 0202-3628

Belayev, A. D.; Miselyuk, E. G.; Slivka, V. Yu.; Turyanitza, I. D. & Chepur, D. V. (1970). On determination of the lattice parameters and Curie points of solid solutions of compounds $A^{V}B^{VI}C^{VII}$, *Ukrainskii Fiz. Zhurnal* 15 (1970) 497-502, ISSN: 0202-3628

Bhalla, A.S.; Newnham, R.E.; Cross, L.E.; Dougherty, J.P. & Smith, W.A. (1981). Pyroelectricity in SbSI. *Ferroelectrics* 33, no.1-4 (1981) 3-7, ISSN: 0015-0193

Cody, G.D.; Tiedje, T.; Abeles, B.; Brooks, B. & Goldstein, Y. (1981). Disorder and the Optical-Absorption Edge of Hydrogenated Amorphous Silicon, *Phys. Rev. Lett.* 47 (1981) 1480-1483, ISSN: 0031-9007

Dittrich, H.; Karl, N.; Kűck, S. & Schock W. (2000), Ternary compounds, organic semiconductors;, In: *Semiconductors, Landolt-Börnstein Condensed Matter III/41E*, Madelung, O. (Ed.), Springer-Verlag, ISBN: 3540667814, Berlin

Dönges, E. (1950). Über Chalkogenohalogenide des dreiwertigen Antimons und Wismuts. I.. Über Thiohalogenide des dreiwertigen Antimons und Wismuts, *Z. anorg. Allg Chem.* vol. 263 (1950) pp. 112-132, ISSN: 0044-2313

Eletskii, A. V. (2004), Sorption properties of carbon nanostructures, *Physics- Uspekhi* 47 (2004) 1119-1154, ISSN: 0038-5670

Entezari, M.H. & Kruus, P. (1996). Effect of frequency on sonochemical reactions II. Temperature and intensity effects, *Ultrason. Sonochem.* 3 (1996) 19-24, ISSN: 1350-4177

Fatuzzo, E.; Harbeke, G.; Merz, W. J.; Nitsche, R.; Roetschi, H. & Ruppel, W. (1962). Ferroelectricity in SbSI, *Phys. Rev.* 127, no 6 (1962) 2036-2037, ISSN: 0031-899X

Fridkin, V.M. (1966). Effects evoked by electron-phonon interaction in phase transition of ferroelectric-semiconductor, *Pisma Zhur. Eksp. Teor. Fiz.* 3 (1966) 252-255, ISSN: 0320-0116

Fridkin, V.M. (1979). *Photoferroelectrics*, Springer-Verlag, ISBN-13: 9780387094182 , New York

Fridkin, V.M. (1980). *Ferroelectric semiconductors*, Consultants Bureau, ISBN: 0306109573, New York

Friedrichs, S.; Falke, U. & Green, M. L. H. (2005), Phase Separation of LaI_3 inside Single-Walled Carbon Nanotubes, (2005). *ChemPhysChem* 6 (2005) 300-305, ISSN: 1439-4235

Gedanken, A. (2004), Using sonochemistry for the fabrication of nanomaterials, *Ultrason. Sonochem.* 11 (2004) 47–55, ISSN: 1350-4177

Gärtner, W. (1957). Spectral distribution of the photomagnetoelectric effect in semiconductors: Theory, *Phys. Rev.* 105 (1957) 823-829, ISSN: 0031-899X

Gerzanich, E.I.; Lyakhovitskaya, V.A.; Fridkin, V.M. & Popovkin, B.A. (1982). SbSI and other ferroelectric $A^{V}B^{VI}C^{VII}$ materials, In: *Current topics in materials science*, vol. 10, Kaldis, E. (Ed.), 55-190, North-Holland, ISBN: 0444863214, Amsterdam

Gomonnai, A.V.; Azhniuk, Yu.M.; Vysochanskii, Yu.M.; Prits, I.P.; Voynarovych, I.M.; Maior, M.M. & Lopushansky, V.V. (2004). Raman scattering in chalcogenide-based ferroelectrics: from bulk to nanoscale, *Phys. Stat. Sol. C* 1, no. 11 (2004) 3166-3169, ISSN: 1862-6351

Gomonnai, A.V.; Voynarovych, I.M.; Solomon, A.M.; Azhniuk, Yu.M.; Kikineshi, A.A.; Pinzenik, V.P.; Kis-Varga, M.; Daroczy, L. & Lopushansky, V.V. (2003). X-ray diffraction and Raman scattering in SbSI nanocrystals, *Mater. Res. Bull.* 38 (2003) 1767-1772, ISSN: 0025-5408

Grekov, A.A.; Korchagina, N.A. & Rogach, E.D. (1979). Clock unit based on ferroelectric device, *Prib. Tekh. Eksp.* 22, no.4 (1979) 262-263, ISSN: 0032-8162

Grigas, J. & Talik, (2003). X-ray photoelectron spectroscopy of ferroelectrics, *Abstracts of 10th European Meeting on Ferroelectrics*, Cambridge U.K. 2003, 143

Grigas, J.; Talik, E. & Lazauskas, V. (2004). X-ray photoelectron spectroscopy of ferroelectric semiconductor SbSI crystals, *Lith. J. Phys.* 44 (2004) 427-438, ISSN: 1648-8504

Grigas, J.; Talik, E. & Lazauskas, V. (2007). X-ray photoelectron spectroscopy of ferroelectrics, *Ferroelectrics* 347 (2007) 86-100, ISSN: 0015-0193

Gruverman, A. & Kholkin, A. (2006). Nanoscale ferroelectrics: processing, characterization and future trends, *Rep. Prog. Phys.* 69 (2006) 2443-2474, ISSN: 0034-4885

Gutiĕrrez, M. & Henglein, A. (1988). Sonolytic decomposition of poly(vinylpyrrolidone), ethanol, and tetranitromethane in aqueous solution, *J. Phys. Chem.* 92 (1988) 2978-2981, ISSN: 0021-9606

Henry son & Garot, D'un produit résultant de l'action réciproque du sulfure d'antimoine et de l'iode, Journal de Pharmacie 10 (1824) 511-24

Hui, Ye.; Yuhuan, Xu. & Mackenzie, J.D. (2000). Semiconducting ferroelectric SbSI quantum dots in organically modified TiO_2 matrix, *Proc. SPIE* 3943 (2000) 95-101, ISSN: 0277-786X

Hui, Ye.; Ligong, Y. & Peifu Gu. (2002). Semiconducting ferroelectric SbSI quantum dots in amorphous matrix: preparation and nonlinear optical properties. *Proc. SPIE* 4918 (2002) 99-104, ISSN: 0277-786X

Ibanez, A.; Jumas, J.C.; Olivier-Fourcade, J.; Philippot, E. & Maurin, M. (1983). On chalcogenide-iodates of antimony SbXI (X=S, Se, Te): structure and Mossbauer spectra of ^{121}Sb, *J. Sol. State Chem.* 48, no.2 (1983) 272-283, ISSN: 0022-4596

Ikemoto, I. (1981). X-ray photoelectroc spectroscopic studies of SbSI, *Bull. Chem. Soc. Jap.* 54 (1981) 2519-2520, ISSN: 1348-0634

Imai, K.; Kawada, S. & Ida, M. (1966). Anomalous pyroelectric properties of SbSI single crystals, *J. Phys. Soc. Japan* 21 (1966) 1855-1860, ISSN: 0031-9015

Irie, K. (1973). Excitation of trapped electrons in SbSI, J. Phys. Soc. Japan 34 (1973) 1530-1535, ISSN: 0031-9015

Irie, K. (1978). Dielectric properties of SbSI, *Ferroelectrics* 21 (1978) 395-397, ISSN: 0015-0193

Ishikawa, K. (1980). Electric field effect on the absorption edge in SbSI, *Japan. J. Appl. Phys.* 19, no.7 (1980) 1301-1309, ISSN: 0021-4922

Ishikawa, K.; Tomoda, W. & Toyota, K. (1984). Crystal growth of SbSI from the vapour phase, *J. Crystal Growth* 69, no.2-3 (1984) 399-403, ISSN: 0022-0248

JCPDS PDF No. 01-072-2366. *Antimony Selenide Sulfide Iodide*

JCPDS PDF No. 01-075-1723. *Antimony Selenide Iodide*

JCPDS Card file 21-0050. *Antimony Iodide Sulfide*

JCPDS Card File 74-0149. *Antimony Sulfide Iodide*

JCPDS Card file 74-1195. *Antimony Sulfide Iodide*

JCPDS Card file 74-1196. *Antimony Sulfide Iodide*

JCPDS Card file 74-2210. *Antimony Sulfide Iodide*

JCPDS Card file 74-2244. *Antimony Sulfide Iodide*

JCPDS Card file 74-2245. *Antimony Sulfide Iodide*

JCPDS Card file 74-2246. *Antimony Sulfide Iodide*

JCPDS Card file 75-0781. *Antimony Sulfide Iodide*

JCPDS Card file 75-1621. *Carbon*

JCPDS Card File 76-1354. *Antimony Sulfide Iodide*

JCPDS Card file 88-0985. *Antimony Sulfide Iodide*

Kikuchi, A.; Oka, Y. & Sawaguchi, E. (1967). Crystal structure determination of SbSI, *J. Phys. Soc. Japan* 23 (1967) 337-354, ISSN: 0031-9015

Kosman, M.S. & Sleptsov, A.I. (1971). Injection currents and accumulation of polarization charge in SbSI, *Fizika Tverdogo Tela* 13, no.10 (1971) 3084-3086, ISSN: 0367-3294

Kotru, S.; Liu, W. & Pandey, R.K. (2000). PLD growth of high vapor pressure antimony sulpho-iodide ferroelectric films for IR applications, ISAF 2000. *Proceedings of the 2000 12th IEEE International Symposium on Applications of Ferroelectrics, IEEE.* Part vol. 1, 2001, pp.231-4 vol. 1. Piscataway, NJ, ISSN: 1099-4734

Kretschmer, R. & Binder, K. (1979). Surface effects on phase transitions in ferroelectrics and dipolar magnets, *Phys. Rev.* B 20 No 3 (1979) 1065-1076, ISSN: 1098-0121

Lebedev, M. V.; Mayer, T. & Jaegermann, W. (2003). Sulfur adsorption at GaAs(1 0 0) from solution: role of the solvent in surface chemistry, *Surf. Sci.* 547 (2003) 171–183, ISSN: 0039-6028

Li, B.; Xie, Y.; Huang, J. & Qian, Y. (1999). Sonochemical synthesis of silver, copper and lead selenides, *Ultrason. Sonochem.* 6 (1999) 217-220, ISSN: 1350-4177

Li, H.-L.; Zhu, Y.-C.; Chen, S.-G.; Palchik, O.; Xiong, J.-P.; Koltypin, Yu.; Gofer, Y. & Gedanken, A. (2003). A novel ultrasound-assisted approach to the synthesis of CdSe and CdS nanoparticles, *J. Sol. State Chem.* 172 (2003) 102–110, ISSN: 0022-4596

Lindsjö, M. (2005). *On The Nature of Main-Group Polycations – An Odyssey*, PhD Thesis, KTH Chemical Science and Engineering, Stockholm 2005

Merz, W.J. & Nitsche, R. (1964). Ferroelectricity in SbSI and other compounds of the group 15-16-17 elements, *Izvest. Akad. Nauk SSSR Ser. Fiz.* 28 (1964) 681-682, ISSN: 0367-6765

Mizukoshi, Y.; Nakamura, H.; Bandow, H.; Maeda, Y. & Nagata, Y. (1999). Sonolysis of organic liquid: effect of vapour pressure and evaporation rate, *Ultrason. Sonochem.* 6 (1999) 203-209, ISSN: 1350-4177

Molnar, B.; Johannes, R. & Haas, W. (1965). Properties of single-crystal SbSI, *Bull. Am. Phys. Soc.* 10 (1965) 109, ISSN: 0003-0503

Moulder, J. F.; Stickle, W. F.; Sobol, P. E. & Bomben, K. D. (1995), *Handbook of X-ray Photoelectron Spectroscopy*, Physical Electronics, Inc., ISBN-13 9780964812413, Chanhassen

Nakonechnyi, Yu.S.; Gorvat, A.A.; Lyakhovitskaya, V.A.; Zadorozhnaya, L.A. & Chapur, D.V. (1979). Low-temperature dielectric anomalies and domain structure in SbSl crystals, *Kristallografiya* 24, no.4 (1979) 793-797, ISSN: 0023-4761

Nitsche, R. & Merz, W. J. (1960). Photoconduction in ternary V-VI-VII compounds, J. Phys. Chem. Solids 13 (1960) 154-155, ISSN: 0022-3697

Nitsche, R.; Roetschi, H. & Wild, P. (1964). New ferroelectric V-VI-VII compounds of the SbSI type, *Appl. Phys. Letters* 4 (1964) 210-211, ISSN: 0003-6951

Nowak, M.; Bober, Ł.; Borkowski, B.; Szperlich, P.; Nowrot, A.; Kępińska, M.; Stróż, D. & Sozańska, M. (2010a). Quantum efficiency coefficient for photogeneration of carriers in SbSI nanowires, send to *J. Phys.: Condens. Matter* (2010), ISSN: 0953-8984

Nowak, M.; Kauch, B. & Szperlich, P. (2009a). Determination of energy band gap of nanocrystalline SbSI using diffuse reflectance spectroscopy, *Rev. Sci. Instrum.* 80 (2009) 046107-1-3, ISSN: 0034-6748

Nowak, M.; Kauch, B.; Szperlich, P.; Jesionek, M.; Kępińska, M.; Bober, Ł.; Szala, J.; Moskal, G.; Rzychoń, T. & Stróż D.; (2009b). Sonochemical Preparation of SbSeI Gel, *Ultrason. Sonochem.* 16 (2009) 546–551, ISSN: 1350-4177

Nowak, M.; Kauch, B.; Szperlich, P.; Stróż, D.; Szala, J.; Rzychoń, T.; Bober, Ł.; Toroń, B. & Nowrot A. (2010b), Sonochemical preparation of $SbS_{1-x}Se_xI$ nanowires, *Ultrason. Sonochem.* 17 (2010) 487–493, ISSN: 1350-4177

Nowak, M.; Jesionek, M.; Szperlich, P.; Szala, J.; Rzychoń, T. & Stróż, D. (2009c). Sonochemical growth of antimony sulfoiodide in multiwalled carbon nanotube, *Ultrason. Sonochem.* 16 (2009) 800-804, ISSN: 1350-4177

Nowak, M.; Mroczek, P.; Duka, P.; Kidawa, A.; Szperlich, P.; Grabowski, A.; Szala, J. & Moskal, G. (2009d). Using of textured policrystalline SbSI in actuators, *Sensors and Actuators* A 150 (2009) 251–256, ISSN: 0924-4247

Nowak, M. & Szperlich P. (2010). Temperature dependence of energy bandgap and spontaneous polarization of SbSI nanowires, send to *Thin Solid Films* (2010), ISSN: 0040-6090

Nowak M.; Szperlich, P.; Bober, Ł.; Stróż, D.; Jesionek, M.; Nowrot, A.; Mistewicz, K.; Starczewska, A. & Kępińska, M. (2010c). Mechanism of sonochemical synthesis of SbSI nanowires, send to *Ultrason. Sonochem.* (2010), ISSN: 1350-4177

Nowak, M.; Szperlich, P.; Bober, Ł.; Szala, J.; Moskal, G. & Stróż, D. (2008). Sonochemical Preparation of SbSI Gel, *Ultrason. Sonochem.* 15 (2008) 709–716, ISSN: 1350-4177

Nowak, M.; Szperlich, P.; Kidawa, A.; Kępińska, M.; Gorczycki, P. & Kauch, B. (2003). Optical and photoelectrical properties of SbSI, *Proc. SPIE* 5136 (2003) 172-177, ISSN: 0277-786X

Nowak, M.; Szperlich, P.; Talik, E.; Szala, J.; Rzychoń, T.; Stróż, D.; Nowrot, A. & Solecka, B. (2010d). Sonochemical preparation of antimony subiodide, *Ultrason. Sonochem.* 17 (2010d) 219-227, ISSN: 1350-4177

Nowak, M.; Talik, E.; Szperlich, P. & Stróż, D. (2009e). XPS analysis of sonochemically prepared SbSI ethanogel, *Appl. Surf. Sci.* 255 (2009e) 7689–7694, ISSN: 0169-4332

Park, S-A.; Kim, M-Y.; Lim, J-Y.; Park, B-S.; Koh, J-D. & Kim, W-T. (1995). Optical Properties of Undoped and V-Doped VA-VIA-VIIA Single Crystals, *Phys. Stat. Sol. B* 187 (1995) 253-260, ISSN: 0370-1972

Park, S.-A.; Yun, S.-H.; Kim, W.-T.; Choe, S.-H. & Kwun, S.-I.(1990). Optical properties of $SbS_{1-x}Se_xI$ and $SbS_{1-x}Se_xI$:Co single crystals, *New Physics* 30 (1990) 763-767, ISSN: 0374-4914

Philips-Invernizzi, B.; Dupont, D. & Caze, C. (2001). Bibliographical review for reflectance of diffusing media, *Opt. Eng*. 40 (2001) 1082-1092, ISSN: 0091-3286

Pipinys, P.; Lapeika, V. & Audzijonis, A. (2004). Electronic Conduction Model in Ferroelectrics Based on Phonon-Assisted Tunneling Emission, *Ferroelectrics* 313 (2004) 91-98, ISSN: 0015-0193

Popik, Yu. V. & Betsa, V.V. (1988). Electronic state of the surface and local levels in SbSI single crystals, *Fizika Tverdogo Tela* 30, no.5 (1988) 1282-1288, ISSN: 0367-3294

Popolitov, V. I. & Litvin, B. N. (1970). Synthesis of ternary chalcohalides $A^{V}B^{VI}C^{VII}$ single crystals, In: *Investigations of Crystallization Processes under Hydrothermal Conditions*, Lobachev, A. N. (Ed.), 55-68, Nauka, Moscow

Popolitov, V. I. ; Litvin, B. N.; Lobachev, A. N.; Yurin, V.A. & Agal'tsov, L.A. (1969). Hydrothermal synthesis and ferroelectric properties of SbSI crystals, *Izvest. Akad. Nauk SSSR Ser. Fiz.* 33, No 2 (1969) 341-343, ISSN: 0367-6765

Pouga, G. D.; Pouga, P. P.; Maksimetz, V. V.; Boretz, A. N.; Hroshik, I. I.; Bercha, D. M. & Chepur, D. V. (1973). Optical and dielectric properties of semiconductor-ferroelectrics $SbS_xSe_{1-x}I$, *Ferroelectrics* 6, no.1-2 (1973) 111-113, ISSN: 0015-0193

Rittenmyer, K.M.; Alexandrakis, G.C. & Dubbelday, P.S. (1988). Detection of fluid velocity and hydroacoustic particle velocity using a temperature autostabilized nonlinear dielectric element (TANDEL). *J. Acoust. Am. Soc.* 84, no.6 (1988) 2002-2006, ISSN: 0001-4966

Samara, G.A. (1975). Effects of pressure on the dielectric properties of and the vanishing of the ferroelectricity in SbSI, *Ferroelectrics 9*, no.3-4 (1975) 209-219, ISSN: 0015-0193

Scott, J.F. (2006).Nanoferroelectrics: statics and dynamics, *J. Phys.: Condens. Matter* 18 (2006) R361–R386, ISSN: 0953-8984

Spitsyna, V. D.; Lyakhovitskaya, V. A. & Belyaev, L. M. (1975). Isomorphous replacement in SbSI, *Kristallografiya* 20 (4) (1975) 840-842, ISSN: 0023-4761

Starczewska, A.; Wrzalik, R.; Nowak, M.; Szperlich, P.; Bober, Ł.; Szala, J.; Stróż, D. & Czechowicz, D. (2008). Infrared spectroscopy of ferroelectric nanowires of antimony sulfoiodide, *Infrared Physics & Technology* 51 (2008) 307-315, ISSN: 1350-4495

Starczewska, A.; Wrzalik, R.; Nowak, M.; Szperlich, P.; Jesionek, M.; Moskal, G.; Rzychoń, T.; Szala, J.; Stróż, D. & Maślanka P. (2009). Influence of the solvent on ultrasonically produced SbSI nanowires, *Ultrason. Sonochem.* 16 (2009) 537–545, ISSN: 1350-4177

Suslick, K.S.; Hammerton, D.A. & Cline, Jr. R.E. (1986), The Sonochemical Hot Spot, *J. Am. Chem. Soc.* 108 (1986) 5641-5642, ISSN: 0002-7863

Szałajko, M. & Nowak, M. (2007). Quantum efficiency coefficient for photogeneration of carriers in gallium sulphide single crystals, J. Phys.: Condens. Matter 19 (2007) 196210, ISSN: 0953-8984

Szperlich, P.; Nowak, M.; Bober, Ł.; Szala, J. & Stróż, D. (2009). Ferroelectric properties of ultrasonochemically prepared SbSI ethanogel, *Ultrason. Sonochem.* 16 (2009) 398–401, ISSN: 1350-4177

Toyoda, K. (1986). Electrical properties of SbSI crystals in the vicinity of the ferroelectric Curie point, *Ferroelectrics* 69, no.3-4 (1986) 201-215, ISSN: 0015-0193

Toyoda, K. & Ishikava, J. (1970). Transport phenomena in SbSI, *J. Phys. Soc. Japan* 28 Suppl. (1970) 451-453, ISSN: 0031-9015

Turjanica, I. D.; Nejezchleb, K. & Horak, J. (1969). Some optical, photoelectric and ferroelectric properies of mixed crystals $SbS_xSe_{1-x}I$, *Czech. J. Phys. B* 18 (1969) 1465-1467, ISSN: 0011-4626

Voutsas, G. P. & Rentzeperis, P. J. (1982). The crystal structure of antimony selenoiodide, SbSeI, *Z. Kristallogr.* 161 (1982) 111-118, ISSN: 0044-2968

Voutsas, G. P. & Rentzeperis, P. J. (1986). The crystal structure of the quaternary compound $SbSe_{0.75}S_{0.25}I$, *Z. Kristallogr.* 178 (1986) 289-295, ISSN: 0044-2968

Voynarovych, I.M.; Gomonnai, A.V.; Solomon, A.M.; Azhniuk, Yu.M.; Kikineshi, A.A.; Pinzenik, V.P.; Kis-Varga, M.; Daroczy, L. & Lopushansky, V.V. (2003). Characterization of SbSI nanocrystals by electron microscopy, *J. Optoelectron. Adv. Mater.* 5, no 3 (2003) 713-718, ISSN: 1454-4164

Wang, C.R.; Tang, K.B.; Yang, Q.; Hai, B.; Shen, G.Z.; An, C.H.; Yu, W.C. & Qian, Y.T. (2001). Synthesis of novel SbSI nanorods by hydrothermal method, *Inorg. Chemi. Commun.* 4, no 7 (2001) 339-341, ISSN: 1387-7003

Wemple, S.H.; Kahng, D. & Braun, H.J. (1967). Surface barrier diodes on semiconducting $KTaO_3$, *J. Appl. Phys.* 38 (1967) 353-359, ISSN: 0021-8979

Xia, Y.; Yang, P.; Sun, Y.; Wu, Y.; Mayers, B.; Gates, B.; Yin, Y.; Kim, F. & Yan, H. (2003). One-Dimensional Nanostructures: Synthesis, Characterization, and Applications, *Adv. Mater.* 15 (2003) 353-389, ISSN: 0935-9648

Yuhuan Xu.; Cheng, C.-H.; Hui, Ye. & Mackenzie, J.D. (2001). Electro-optic effect in a nano-crystals doped glass, *Ferroelectrics* 259 (1-4) (2001) 259-68, ISSN: 0015-0193

Yuhuan, Xu.; Del Monte, F.; Mackenzie, J.D.; Namjoshi, K.; Muggli, P. & Joshi, C. (1999). Nanocomposite of semiconducting ferroelectric antimony sulphoiodide dot-doped glasses, *Ferroelectrics* 230 (1-4) (1999) 11-20, ISSN: 0015-0193

Yun, W. S., Urban, J. J.; Gu, Q. and Park, H. (2002). Ferroelectric Properties of Individual Barium Titanate Nanowires Investigated by Scanned Probe Microscopy, *Nano Letters* 2, no 5 (2002) 447-450, ISSN: 1530-6984

Zeinally, A.Kh.; Agasiev, A.A. & Efendiev, Sh.M. (1974). Direct 'allowed' transitions in SbSI, *Fiz. Tekhn. Poluprovod.* 8, no.1 (1974) 197-200, ISSN: 0015-3222

Zhdan, A.G. & Artobolevskaya, E.S. (1971). Properties of contacts between SbSI single crystals and some metals. Fizika Tverdogo Tela 13, no.4, (1971) 1242-1244

Žičkus, K.; Audzijonis, A.; Batarūnas, J. & Šileika, A. (1984). The fundamental absorption edge tail of ferroelectric SbSI. *Phys. Stat. Sol. B* 125, no.2 (1984) 645-651, ISSN: 0370-1972



Nanowires Science and Technology

Edited by Nicoleta Lupu

ISBN 978-953-7619-89-3
Hard cover, 402 pages
Publisher InTech
Published online 01, February, 2010
Published in print edition February, 2010

This book describes nanowires fabrication and their potential applications, both as standing alone or complementing carbon nanotubes and polymers. Understanding the design and working principles of nanowires described here, requires a multidisciplinary background of physics, chemistry, materials science, electrical and optoelectronics engineering, bioengineering, etc. This book is organized in eighteen chapters. In the first chapters, some considerations concerning the preparation of metallic and semiconductor nanowires are presented. Then, combinations of nanowires and carbon nanotubes are described and their properties connected with possible applications. After that, some polymer nanowires single or complementing metallic nanowires are reported. A new family of nanowires, the photoferroelectric ones, is presented in connection with their possible applications in non-volatile memory devices. Finally, some applications of nanowires in Magnetic Resonance Imaging, photoluminescence, light sensing and field-effect transistors are described. The book offers new insights, solutions and ideas for the design of efficient nanowires and applications. While not pretending to be comprehensive, its wide coverage might be appropriate not only for researchers but also for experienced technical professionals.

How to reference

In order to correctly reference this scholarly work, feel free to copy and paste the following:

Marian Nowak (2010). Photoferroelectric Nanowires, Nanowires Science and Technology, Nicoleta Lupu (Ed.), ISBN: 978-953-7619-89-3, InTech, Available from: http://www.intechopen.com/books/nanowires-science-and-technology/photoferroelectric-nanowires

INTECH
open science | open minds

InTech Europe
University Campus STeP Ri
Slavka Krautzeka 83/A
51000 Rijeka, Croatia
Phone: +385 (51) 770 447
Fax: +385 (51) 686 166
www.intechopen.com

InTech China
Unit 405, Office Block, Hotel Equatorial Shanghai
No.65, Yan An Road (West), Shanghai, 200040, China
中国上海市延安西路65号上海国际贵都大饭店办公楼405单元
Phone: +86-21-62489820
Fax: +86-21-62489821

© 2010 The Author(s). Licensee IntechOpen. This chapter is distributed under the terms of the Creative Commons Attribution-NonCommercial-ShareAlike-3.0 License, which permits use, distribution and reproduction for non-commercial purposes, provided the original is properly cited and derivative works building on this content are distributed under the same license.

IntechOpen

IntechOpen